



AUTHOR(S):

TITLE:

YEAR:

Publisher citation:

OpenAIR citation:

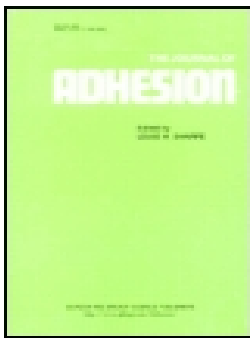
Publisher copyright statement:

This is the _____ version of an article originally published by _____
in _____
(ISSN _____; eISSN _____).

OpenAIR takedown statement:

Section 6 of the "Repository policy for OpenAIR @ RGU" (available from <http://www.rgu.ac.uk/staff-and-current-students/library/library-policies/repository-policies>) provides guidance on the criteria under which RGU will consider withdrawing material from OpenAIR. If you believe that this item is subject to any of these criteria, or for any other reason should not be held on OpenAIR, then please contact openair-help@rgu.ac.uk with the details of the item and the nature of your complaint.

This publication is distributed under a CC _____ license.



Acoustic emission method to study fracture (Mode-I, II) and residual strength characteristics in composite-to-metal and metal-to-metal adhesively bonded joints

Mohamad Ghazi Droubi, Alan Stuart, John Mowat, Craig Noble, Anil Kumar Prathuru & Nadimul Haque Faisal

To cite this article: Mohamad Ghazi Droubi, Alan Stuart, John Mowat, Craig Noble, Anil Kumar Prathuru & Nadimul Haque Faisal (2017): Acoustic emission method to study fracture (Mode-I, II) and residual strength characteristics in composite-to-metal and metal-to-metal adhesively bonded joints, The Journal of Adhesion, DOI: [10.1080/00218464.2017.1278696](https://doi.org/10.1080/00218464.2017.1278696)

To link to this article: <http://dx.doi.org/10.1080/00218464.2017.1278696>



Accepted author version posted online: 12 Jan 2017.



Submit your article to this journal [↗](#)



Article views: 15



View related articles [↗](#)



View Crossmark data [↗](#)

Acoustic emission method to study fracture (Mode-I, II) and residual strength characteristics in composite-to-metal and metal-to-metal adhesively bonded joints

Mohamad Ghazi Droubi, Alan Stuart, John Mowat, Craig Noble, Anil Kumar

Prathuru, Nadimul Haque Faisal¹

School of Engineering, Robert Gordon University, Garthdee Road, Aberdeen, AB10 7GJ, UK

Abstract

Failure behaviour of two types of adhesively bonded joints (composite-to-metal, metal-to-metal) has been studied under failure modes (Mode I: double cantilever beam (DCB) and Mode II: three-point end notch flexures (3-ENF)) using acoustic emission (AE) technique. The bonded specimens were prepared using two types of adhesive bond materials with three variations of adhesive bond quality. The effect of the presence of interfacial defects along the interface on the residual strength of the joint has also been studied. It was possible using the maximum AE amplitude method to select the AE events of mechanical significance. However, it proved difficult to propose a definitive AE trait for the mechanical phenomena occurring within specific AE event signals, for all adhesive types, bond qualities, and substrate configurations; therefore, all specimen combinations. There was a notable shift in spectral energy proportion as the AE source of mechanical significance varied along the specimen length for specimen combinations. However, it was difficult to confirm this distinctive trait for all specimen combinations due to difficulty in confirming the location and exact mechanical source. The proposed measurement technique can be useful to assess the overall structural health of a bonded system and may allow identification of defects.

¹ Corresponding authors. E-mail addresses: N.H.Faisal@rgu.ac.uk; Tel: +44 (0) 1224-26 2438.

Keywords: adhesive materials, destructive testing, fracture mechanics, failure modes (Mode-I, II), interfacial fracture, acoustic emission, residual strength.

1. Introduction

As per Standard Terminology of Adhesives (ASTM D907-15) [1], ‘adhesive joint failure’ is defined as the ‘locus of fracture occurring in an adhesively-bonded joint resulting in a loss of load-carrying capability’ and therefore ‘residual strength’ can be defined as the loss of load-carrying capability. The strength of an adhesive joint depends on several factors such as the elastic properties of the adherends and that of the adhesive, type of the joint (lap, scarf, butt, etc.), surface preparation, geometry of the joint, type of loading, dimensions of the joint, uniformity of the bond line, thickness of the bond line, homogeneity of the cured adhesive etc. The failure in an adhesive joint mostly happens in the weakest link i.e. adhesive or contacting surface.

The Mode-I failure mechanism most relates with the cleavage loading type, with a tensile stress normal to plane of crack. This mode can be established through various testing methods such as the double cantilever beam (DCB), tapered-double cantilever beam (T-DCB) and Boeing wedge (BW). Chaves et al. [2] state that the DCB is most highly regarded of the Mode-I test methods. The DCB experimental method induces the adhesive Mode-I fracture mechanics by pulling the two substrates apart at one end using a tensile testing machine, including suitable reference to the ISO 25217:2009 standards [3]. A contrast between two different Mode-I testing methods was conducted by Adams et al. [4] who compared the BW against the DCB and formed the conclusion that the DCB equations are the simpler of the two. However, Adams et al. [4] concluded that the DCB produced a high uncertainty of results through initial procedure due to rapid propagation of crack following opening load.

Contrasting the conclusions of Adams et al. [4], Ducept et al. [5] found no uncertainty in the initial crack propagation of the DCB results.

The rich surplus of experimental procedures concerning the Mode-I failure type over the years, in comparison to the other modes, has generated strong foundations for further investigation. Mode-I, taking the form of a cleavage fracture mechanics, creates a lower fracture resistance from the two modes being tested in the current study (Mode-I and -II). Ranade et al. [6] used a DCB configuration with bolted end-blocks and thus eliminated the additional uncertainty added through the elastic properties of an adhesive. This produced results that proclaimed an ideal bondline thickness would produce the highest fracture energy. Constante et al. [7] discussed the same phenomenon where it was termed as cohesive law. The use of the bolted end-blocks in Ranade et al. [6] study may be highly considered in the current study to help reduce any further possible AE sources. Hasegawa et al. [8] stated that the highest fracture energies created by the DCB method are created by cohesive failure for DCB experiments while using a constant bondline thicknesses and composite substrates, with de Morais [9] considering pre-crack adjustment on steel substrates using finite element (FE) analysis. The graphical analysis in de Morais [9] study showed a steep decrease in fracture energy with increased pre-crack length before showing signs of settling. This phenomenon was found to most likely occur due to increased leverage with greater pre-crack length and hence reduced the force required to fracture the adhesive bond. Papini et al. [10] experimented with variance of loading rate using a DCB set-up and concluded that the displacement rate directly relates to the energy release rate of the fracture. Slower loading rates attained data closer to the anticipated results from DCB calculations. Recent innovations in DCB testing conducted by Campilho and da Silva [11] measured fatigue and fracture behaviour of carbon fibre-reinforced polymer (CFRP) DCB joints. They established milling tools to be insufficient for composite substrates and also found that the visibility of crack

propagation is vital in evaluation of final results and conclusions. Forte et al. [12] also highlighted the risk of substrate failure occurring through this experimental method when using composite substrates due to the material configuration against the method of loading. The rapid crack growth of DCB testing relates to the substrate type (i.e. dependant on the elastic region of utilised material). This can be accounted for through alteration of the rate of crosshead displacement ranging from 0.1 mm/min [6] to 2 mm/min [13]. This factor can be linked with the dimensions of the substrates, however ISO 25217:2009 [3] standards regarding Mode-I adhesive (DCB/T-DCB) testing provide appropriate guidance specifying a displacement rate range for both substrate material types; metallic = 0.1-0.5 mm/min, fibre-composite = 1.0-5.0 mm/min.

The Mode-II failure mechanism relates to the shear loading, with high performance composites designed to have great in-plane stiffness and strength, as investigated by Chaves et al. [2]. This mode of failure can be established through 3-ENF, 4-ENF, and End Load Split (ELS). This failure mechanism presents the highest resistance to fracture of the two Modes investigated in the current study. The 3-ENF is the preferred method of testing Mode-II fracture toughness; whereas the 4-ENF was found to feature excessive frictional properties [14-15]. The 3-ENF method provides a single point moving force on one side of a substrate, and two reaction forces on the other.

The Mode-II fracture mechanics are determined by loading a specimen by in-plane shear and require further research due to the designed nature of adhesive joints [15]. As mentioned above, the Mode-I loading has a lesser fracture resistance in comparison to Mode-II, therefore specimens are engineered to favour reduction of this loading and hence promote Mode-II loading [17]. However, the debate over the standardisation of Mode-II failure testing has been on-going over the years. Martin and Davidson [18] originally proposed the 4-ENF test as an alternative to 3-ENF, however, Schuecker and Davidson [14-15] found that the

application of the 4-ENF test presented difficulties due to large frictional effects and de Moura et al. [19] further discussed the complex methodology of the 4-ENF experiment. Blackman et al. [16] found that the nature of the ELS fixture and the clamping creates an uncertainty in boundary conditions (BC's) and hence unreliable data, which arises complications in correcting the data. Russell and Street [20] originally devised the 3-ENF experimental procedure that was found to be simple to analyse, however, the crack propagation was found to be inconsistent without first implementing a large length of pre-crack. Yang et al. [21] proved through demonstration the possibility of numerically predicting the loads associated with crack growth and to model the plastic deformation of adhesive joints with a shear loading. However, de Moura et al. [19] developed a methodology for characterising ductile adhesive layers under pure Mode-II fracture mechanics in bonded joints. The discussed conclusions by Shuecker and Davidson [14-15] concerning excessive frictional effects of the 4-ENF method, gave appropriate reasoning when considering these effects on the AE signals created through testing in current study.

This study therefore aims to characterise the failure behaviour of two types of adhesively bonded specimen (e.g. composite-to-metal and metal-to-metal) under failure modes namely Mode I: double cantilever beam (DCB) and Mode II: three-point end notch flexures (3-ENF) using the acoustic emission (AE) monitoring technique. AE may aid in the understanding of the mechanics behind the specified failure modes of adhesively joined composite structures. Different combinations of specimens were tested with multiple varying parameters such as material combination, adhesive type and adhesive bond quality.

2. Materials and methods

2.1 Adherend materials

Carbon fibre composite sheets of average thickness 1.35 mm were created using a resin infusion method. This process involved six layers of pre-woven carbon fibre were cut

into sections roughly 350 mm x 250 mm. The 2-part epoxy resin was drawn through the layers using a vacuum suction method. An infusion spiral and mesh allowed the resin to disperse evenly throughout the layers. This setup was left for 1 week before the layers were cut into multiple specimens of 200 mm x 25.4 mm. The metallic substrates were manufactured using EN AW-6082/T2, 25.4 x 6.35 x 5000 mm aluminium alloy (Aalco Metals Ltd, Surrey, UK) bar which was cut using a milling machine to length just over the designated specimen length. To bolt the end-blocks, four holes with 3 mm diameter were drilled in the appropriate locations and countersunk using a milling machine. The end-blocks were manufactured using a 20 x 20 mm steel 'black bar', which was dimensioned in the same manner as the aluminium substrates, using a milling machine to ensure an accurate and square profile. 2.5 mm holes were drilled and tapped using a 3 mm tap. A 3 mm x 20 mm stainless steel countersink screws were used to secure the end-block to substrate.

2.2 Adhesive bond materials

The adhesive bonds between the substrates were achieved through a process of surface preparation, adhesive activation, adhesive application, and uniform force application between substrates. Following the surface preparation (i.e. cleaning using Loctite® SF 7063™ [Henkel Ltd., Hemel Hempstead, UK]), the application of the Loctite® 7649™ (Henkel Ltd., Hemel Hempstead, UK) activator was applied to the surface of the specimens and let to air dry. At this stage, Rocol® Dry PTFE Spray (Rocol, Leeds, UK) (which is insoluble in solvents, does not easily transfer) was used to act as a pre-crack, a length of 140 mm (out of 200 mm length) was covered so the remaining length was generously coated with the spray. The pre-crack was only applied to one substrate. If the bond quality had to be applied, the use of Dry PTFE Spray was evenly sprayed through the templates, and left to dry until the residue was visible. Once dry, either brittle adhesive, transparent Loctite®

EA3430TM (Henkel Ltd., Hemel Hempstead, UK), a 2-component epoxy adhesive system, or ductile adhesive, transparent and yellow to light amber Loctite® AA326TM (Henkel Ltd., Hemel Hempstead, UK), a 2-step acrylic adhesive, was used to apply the 250 µm shims used to keep a consistent adhesive thickness. The opposite specimen was then carefully and accurately placed on top, ensuring the 6 mm holes were aligned correctly. A 3 kg weight was then placed on a flat plate that spanned across 3 specimens and left for 1 week to cure, without being disturbed. The blocks for the composite specimens were then attached using tough epoxy adhesive, white opaque Loctite® EA9466TM (Henkel Ltd., Hemel Hempstead, UK). This adhesive was used due to the greater tensile and peel strengths than either of the other adhesives (Loctite® EA3430TM, Loctite® AA326TM [Henkel Ltd., Hemel Hempstead, UK]). The blocks also had the 3 kg brass mass placed across them to ensure the best possible bond, so the adhesive between the substrates would fail first. The end-blocks for the composites were attached to the rougher side of the substrate; the end-blocks were attached only with abrasion to the block and not the substrate itself. No shims were used for maintaining thickness between the block and substrate. Furthermore, all individual specimen combinations were cured under the following average conditions, which were measured using a traceable hygrometer (Fisher Scientific UK Ltd., Loughborough, UK). One side of the specimen was painted with a white non-solvent based paint (Hammerite), to enable more visible fracture propagation.

2.3 Bond area control

Adhesive bonding area was investigated through three levels of control; 100%, 75% and 65% of the bonded surface area. To maintain a constant reduction in the bond quality, the design and manufacture of quality control templates was required. It is expected that due to large scale production of bonded joints in industrial process, the adhesive material may not

bond completely with the adherends, leading to a reduced adhesion quality. Therefore, the template method has been proposed in this work to simulate the effect of reduced bond area at the interface (which can appear either during production or during usage of the bonded specimens), which in effect will reduce the strength of adhesively bonded joints. The template method is appropriate in this investigation as it provides a regular defect pattern and measurable bond area. The templates are shown in **Fig. 1(a)** and were achieved using a Computer Numerical Control (CNC) (Bungard Elektronik, Windeck, Germany) machine to load and cut the design (**Fig. 1(b)**). The circuit boards were then cut to the length (L) of 200 mm and a width (w) of 25.4 mm after the holes were drilled, as this coincides with the specimen length. The hole diameter used were 3.15 mm (θ_1) and 2.5 mm (θ_2). As shown in **Fig. 1(a,b)**, there are no holes drilled for the pre-crack (PC), for a length of 60 mm, as this will be covered with a non-stick material throughout the adhesion stage. The templates (**Fig. 1(b)**) are placed over the bond-controlled specimen following the surface preparation. This allows a layer of PTFE spray to be applied through the holes onto surface of the specimen substrate.

2.4 Double cantilever beam (DCB, Mode-I) testing

To gain accurate results from the pure Mode-I testing of adhesive bonds, the material type and specimen dimensions (length: 200 mm, width: 25.4 mm, thickness: 6.35 mm, pre-crack: 60 mm) were considered against existing literature into the topic. The choice of aluminium alloy as the metal substrate was decided to be in line with previous work [5, 12, 22]. The specimen dimensions used in previous work [22] were deemed inappropriate and may experience plastic deformation during experimentation; therefore, the specimen thickness was varied between 1.5 mm and 6 mm during material selection analysis. The aluminium alloy was assumed to have the material properties (minimum yield strength: 280

MPa, minimum ultimate tensile strength: 310 MPa, elastic modulus: 95 GPa). The review of the yield strength against the specimen thickness deemed the specimen dimensions and assumed mechanical properties to be sufficient (analysed through ANSYS 14.0 analysis). The metal substrate was AW-3082/T6 aluminium alloy and the assumed mechanical properties were deemed adequate through the EN 10204:3.1 certification as provided by the supplier (Cosmos Aluminium, Longkou City, China).

The DCB setup, shown in **Figs. 2(a)**, which was manufactured for this test includes a rig adaptor (jig) that can be inserted into the tensile test machine (maximum load of 100 kN, maximum crosshead displacement of 1500 mm) (Model 3382, Instron Ltd., High Wycombe, UK) to be pulled apart at a user-defined rate through the BlueHill 3.0 software. From the ISO 25217 [3], it was decided that this investigation would use 0.5 mm/min and 2 mm/min for metal-to-metal and metal-to-composite specimens, respectively. Camera footage enabled the time, load and AE data to be analysed with an image reference to confirm an event had occurred along the adhesive bonding length. The blocks were designed with a central, 6 mm hole to allow free rotation about the neutral axis. This allows the blocks to adjust continuously as the load is applied without any external forces affecting the results, except minimal friction. The height-gap within the jig allows for the designed blocks to have over 270° of movement without the specimens encountering the jig. Two opposing, outward facing sides of the blocks were designed with M3 threaded holes that allow any specimen size smaller than 30 mm in width to be inserted without colliding surfaces; hence designed with reusable purpose. The AE sensor was held in place using electrical ‘earth’ tape (**Fig. 2(a)**) with a layer of RS Component silicon grease applied and positioned in a consistent location for all the tests carried out. Once the testing commences, the ruler along the edge allows for a visual aid of the crack propagation and allows a reference for the camera footage following experimentation, to identify any significant activities that may occur.

2.5 Three-end notch flexure (3-ENF, Mode-II) testing

The 3-ENF setup (**Fig. 2(b,c)**) required the calculation of the bending moments and the yield point of both of the combinations of metal-to-metal and composite-to-metal adhesively bonded specimens. Initially, the force calculated for the metal-to-metal specimens was determined using the following assumptions: homogeneous material properties, negligible thickness of adhesive, the specimen acted as two solid 6.36 mm beam in perfect contact, and the force applied was equivalent throughout the specimen. The bending moments were adapted to give equation ($F=2\sigma_{max,x}bh^2/3L$) and the calculation resulted in a total force of 2014 N before the metal-to-metal specimen yielded. With regards to the metal-to-composite beam, the force to bring the CFRP past the yield or failure point was also calculated. The compound beam equivalent area theory was used for this to allow a direct link between the aluminium and CFRP. Therefore, a modular ratio was calculated alongside a new 2nd moment of inertia for the equivalent free body diagram. Using the bending equation ($M/I=\sigma/y=E/R$), allowed the maximum force of 7.5 kN to be found before breaking point. However, it can be confirmed that by this stage total failure of the aluminium alloy would have occurred within the 3-point bend rig.

2.6 Experimental procedure

Preceding the manufacture of the specimens, WaveMatrix Dynamic and Fatigue Materials Testing Software (Instron Ltd., High Wycombe, UK) was used to program the hydraulic machine (Model 1342, Instron Ltd., High Wycombe, UK) for experimentation. The 3-ENF jigs, shown in **Fig. 2(b)**, were designed and manufactured by Instron to their standard. The bottom rollers were adjusted to 15 mm from each end of the specimen with the top aligned at the 100 mm halfway point. The rollers in this case were free to move within the mount. This ensured only one point of contact on the specimen at any one time, allowing the

calculations carried out in 3-ENF methodology to be related to the bending beam theory. The rate at which the ram would be working was set up through the WaveMatrix software through two control methods for the different specimen combinations. It was decided that this investigation would use -0.5 mm/min and -2 mm/min for metal-to-metal and metal-to-composite specimens, respectively, where the ramping rate value is negative due to ram moving in the upward direction towards the top roller. All the specimen experiments were recorded using a digital camera.

2.7 AE instrumentation

A Micro-80D differential AE sensor with frequency range of 100 – 1000 kHz with 340 kHz resonance frequency (Physical Acoustics Ltd, Cambridge, UK) was used throughout the investigation. Silicone grease was applied to the sensor (to avoid any air gap) before attaching to the specimen surface using electrical tape. The AE sensor was connected to a pre-amplifier (Physical Acoustics Ltd, Cambridge, UK) that was utilised to amplify the acquired signals gain and could be varied (20/40/60 dB). The pre-amplifier was connected to an in-house-built 4-channel signal conditioning unit (SCU) that was coupled with a gain programmer to supply 28V of power, coupled with adjustable gain control. The SCU transmits the adjusted signal to a BNC-2120 shielded connector block (National Instruments, Berkshire, UK) to complete the systems signal transmission to the data acquisition card (DAQ). The signals were interpreted through a computer using a 10 MS/s NI PCI-6115 DAQ (National Instruments, Berkshire, UK) to obtain the raw signal data and convert it to a binary file within the LabVIEW software for further analysis using MATLAB. The AE sensor was placed at the top surface all tested samples, as it was placed for all of the experiments carried out in this study and ten consecutive pencil lead break (Hsu-Neilsen PLB source [23-24]) tests were conducted at 20 mm increments from the AE sensor along the length of the

specimens (see **Fig. 2(d)**), which allow a correlation to be drawn between AE energy with distance from a sensor. AE signal acquisition for the mechanical testing of the specimens were set at (SCU gain: 20 dB, Pre-amp gain: 12 dB, sampling frequency: 2.5 MHz, acquisition time: 1 s).

2.8 Specimens and coding

In the current investigation, a unique specimen for each test has been manufactured, and adhesive thickness has been kept consistent (i.e. 250 μm) for all tested specimens and was not considered among the variables in this study. Systematic coding has been employed to allow an effective means of communicating individual specimen types and their representative data in the following discussion section. **Table 1** presents the coding system and an example of the system has been provided as follows: DCB.MM.D.100.

3. Results and discussion

3.1 Calibration and AE signal characteristics

AE propagation characteristics was first determined using a large cylindrical steel block of dimension 200 mm diameter and 150 mm height to provide a reference calibration. PLB were carried out on each MM specimens, MC specimens, MM un-bonded interface, MC un-bonded interface, single metal substrate surface and single composite substrate surface. The recorded AE energy for the ten pencil lead breaks at all positions was represented by average AE energy points along with their standard deviation and used in the following general analysis. The AE energy relationship identified from the calibration block testing can be confirmed for the MM specimens used in the investigation (see **Fig. 3(a)**), although further trends are identifiable. The AE energy generated by a PLB on a single metal substrate surface was found to be lower than that of the MM un-bonded interface; therefore, the acoustic

attenuation of an AE source can be lessened with un-bonded, contacting interfaces. In addition, it was found that introducing a bonded interface may decrease the acoustic attenuation at distances where the AE source is in the near vicinity of the AE sensor (approximately 40 mm). However, the improvement in acoustic attenuation was not identified where the AE source was at greater distances from the sensor (approximately 60 mm). The adhesive bond area (or quality) was found to be irrelevant to the acoustic attenuation of the different specimens when the curing process was uniform and complete. It can be seen from **Fig. 3(a)** that the AE energy at the increasing distances from the sensor, remains consistently similar, even when considering the error band of standard deviation. However, it was noted that the PLB testing of the ductile adhesively bonded specimens produced interesting results (**Fig. 3(b)**), which did not correlate well with the brittle adhesively bonded specimens (**Fig. 3(a)**). The trends found in the MM.D specimens were determined to have been a result of the unperfected, initial bonding process where there were some discrepancies that are further discussed. **Figure 3(c)** shows post-experimental inspection of a MM.D specimen. Nayeb-Hashemi and Rossettos [25] found no direct correlation between attenuation change and bond strength for adhesively bonded specimens featuring internal disbond's, however identified a correlation for specimens featuring voids. These findings can be related to **Fig. 3(c)**, where voids were detected and notable change in attenuation was found as the AE source was altered along the specimen length.

Again, the AE energy generated by a PLB on a single composite substrate surface was found to be lower than that of the MC un-bonded interface; however, featuring an order of magnitude lesser than MM unbounded interface. In addition, this furthers the conclusion that acoustic attenuation of an AE source can be lessened by introducing metal or composite as a contacting interface. Limited AE energy trend similarities were identified between the different bonding qualities for these specimens. However, no direct conclusions can be drawn

between these specimens from the acquired calibration data. The trend obtained from the MC.B.65 specimen was determined to have relation to voids, as identified with specimen MM.D.65 (see **Fig. 3(c)**). However, MC.B.75 was noted to have AE energy with magnitude that was comparable with a single composite specimen and may suggest large void presence throughout the whole specimen. The MC.B.100 trend agreed with the findings of the MM.B PLB testing, where acoustic attenuation was improved in the near vicinity of the AE sensor (approximately 40 mm), whilst AE energy maintained rather consistent levels with the specimen featuring no adhesive. The difference in AE energy from the AE source was deemed to be due to the damping of the AE signal, induced by the composite specimen.

A comparison of the difference between the AE signal duration of the metal and composite substrates was drawn in **Figs. 4(i,ii)**, where identical window lengths and y-axis scaling were used to highlight the difference. It was also noted that the frequency spectrums were orders of magnitude different and the metal substrate seemed to have large spectral energy at higher frequencies than the composite specimen. Again, this was deemed to be related to the high damping of the AE signal in the composite specimen. Identification of the frequency spectrums of the specimen combinations would allow further differentiation to be seen in the further experimentation. The PLB AE responses were processed, analysed and it was found that there was high spectral energy content at frequencies lower than 400 kHz; however, were notably smaller in content in comparison with the frequencies higher than 400 kHz (see **Fig. 4(iii)**). Therefore, it was deemed appropriate to note the difference in significant spectral energy content and the complete range of frequency spectrum between the specimen combinations (see **Table 2** and **Table 3**). It was noted that frequency spectrums (and hence the spectral energy) differed along the distance of the specimen. This was expected as the location of the AE source would change, the acoustic waves would transmit through the material differently; and hence the frequency and strength of the received

acoustic wave would differ. Therefore, the distance from the sensor should be taken into consideration when analysing the AE responses acquired for the mechanical testing of the specimens.

3.2 Double cantilever beam (DCB, Mode-I)

3.2.1 Detection of plastic deformation

In accordance to the ISO 25217:2009 (Mode-I opening load, using DCB) [3], an appropriate measure of plastic deformation requires visual inspection of substrates following the test procedure. Post-experimentation comparison of the substrates against a steel rule allowed clarification that no plastic deformation had occurred during experimentation. All specimens succeeded in resisting plastic deformation, validating simulation discussed in previous section, and ensuring accuracy of DCB experimentation.

3.2.2 Loading graphs

The loading output plots of the DCB experimentation were divided into three identified phases of mechanical significance. Both the ductile and brittle adhesives were divided accordingly: initial pre-crack extension of the specimen (I), elastic region of the substrate and adhesive (II), and the adhesive de-bonding to the final adhesive failure (III). **Figure 5(a)** shows the different phases of the DCB specimen failure to be discussed accordingly in regards to the AE produced, with visible boundaries dividing these stages. Phase I indicate the initial loading of specimen along the pre-crack extension, during this phase there is no elastic deformation of the substrate and the pre-crack is widening. The boundary between Phase I and II signifies the loading reaching the interface between the pre-crack and the fully bonded adhesive, the latter of which becomes under stress. Phase II represents the combined elastic deformation of the substrate and adhesive, as they experience

stress due to the resistance from adhesive bonding, where Benmedakhene et al. [26] agree with this. The boundary between Phase II and III represents a yielding as the loading exceeds the yield strength of the adhesive bond, and de-bonding initiates until final failure, as shown in Phase III with similar phases presented in Bohse [27] and Senthil et al. [28] studies. The inconsistent profile found within the de-bonding region (Phase III) could be a result of slight differences in adhesive thickness, properties and curing circumstances; these factors have been minimised (see *Section 2.4*), however are extremely difficult to limit. There was potential for non-uniform abrasion of the specimen surface, therefore surface contaminants may have remained present and hence cause inconsistency between individual substrates, where the importance of the roughness was discussed by Boutar et al. [29]. Following the more thorough abrasion, the specimen could be completely submerged within a diluted acid bath or acetone and be subject to a rinsing with distilled water and air dry, where the noticeable effect of the cleaner on bond quality was also discussed to be tested by Schleikermann [30].

Following the surface preparation, PTFE was used to apply the pre-crack and any bond qualities, if required. The length of the pre-crack may have featured slight variation due to the technique used to expose the pre-crack area. It has been identified that the pre-crack location may be a good indicator for consistent frequency spectrum response upon the initial adhesive failure, therefore it may be vital to maintain minimal variation in the pre-crack length. Application of the PTFE through a quick curing liquid would allow a precise, consistent quantity for each individual specimen. The use of the activator was similar to the pre-crack, where an exact volume of area coverage was not guaranteed from repetition of each specimen. A large source of error may be sourced from the irregularity between adhesive thickness throughout the individual specimen and between specimen combinations. The shims were positioned to control the adhesive thickness to 250 μm , however, it was

identified that the bonded thickness varied between individual specimen combinations (metal-adhesive-metal: average total thickness of 13.32 mm, which includes about 605 μm adhesive average thickness; metal-adhesive-composite: average total thickness of 8.31 mm, which includes about 597 μm adhesive average thickness). This was due to the shims being glued into place therefore, the thickness below and above the shims changed and therefore the overall thickness altered. An excess of the adhesive was applied to ensure complete area coverage of the individual specimen; hence following load application, there were visible excess exiting from between the substrate at the edges. The thickness consistency of the specimen could be achieved through a simple spreading component that would run back and forth across the specimen length at a user-determined height. However, this component would require a high level of accuracy design to achieve the desired consistency. Linking this alongside the use of the shim technique may allow for definitive consistency during the adhesive application process. The specimens were left to cure within the same enclosed environment (fumigation cupboard) at room temperature. However, this may have resulted in different adhesive curing against the specified conditions stated in the data sheets. The adhesive strength modulus is seen to decrease with increased humidity, in accordance to Chang et al. [31] study. The specimens could be cured within a pressure or temperature chamber, which would allow for a more in-line method of curing with the adhesive specifications'. The manual nature of the manufacturing process introduced human error, where the same process was repeated twelve times throughout to produce each mode of failures' specimen. To maintain consistency, the same procedure was followed and the same personnel made the specimens. Although the same procedure was followed, human error may have factored more heavily initially, where the procedure became more familiar in each proceeding specimen batch, as seen in the DCB.MM.D specimen (see *Section 3.1*).

The three phases were verified photographically, as this allows for the breakdown of results and further analysis. The MM.D results show similar trends for all three of the bond area (qualities), however display different loading gradients within Phase I compared to Phase II. From the camera footage of the experiments, it was seen there was an initial failure of pre-crack displayed, which correlates to the initial steep loading rate in Phase I. This load gradient is then reduced due to the elastic deformation of the substrate in Phase II, with relating photographic evidence showing the initial failure up to 60 mm. The load then gradually drops until a sudden and final failure occurs, where video footage showed the crack propagation along the specimen length. The DCB.MM.B was the only MM specimen to show a significant level of stick-slip throughout the failure.

Figure 5(b) shows the sudden de-bonding and attachment between the cured and uncured sections of the specimen as shown in *Section 3.1*. This specimen, although regarded incorrect in recording crack propagation by ISO 25217:2009 [3] standards, was still considered when analysing AE data, where conclusions could still be made regarding the uncured properties of the adhesive. The stick-slip phenomenon could be due to insufficient bonding procedures through the specimen manufacturing stage of the project discussed previously. The MM.B specimens all showed the same trend with an initial load throughout Phase I, with again a subsequent reduced loading gradient, showing indication of Phase II. Phase III signifying the de-bonding process showed smaller initial failures than the ductile adhesive and feature a final notable load drop representing catastrophic failure; these three phases are compared in **Fig. 5(c)**. The DCB.MM.B.65 showed more of a gradual curve towards final failure before a small catastrophic failure, where this result could be due to the bond quality initiating a more steady adhesive de-bonding process. Comparison between the MM.D and MM.B specimens indicates that complete failure of MM.D specimens occurs over a greater amount of time. This could be due to the greater elastic, ductile properties of the

adhesive itself, although the failure occurring at a lower load. Visual de-bonding shown on the brittle loading graph is also less varying than that of the ductile adhesive, with fewer recognisable points of de-bonding. The MC specimens were loaded at an accelerated loading rate of 2 mm/min to compensate for the carbon fibre composite's flexure properties, in accordance with ISO 25217:2009 [3] standards. The MC tests showed similar phases (see **Fig. 5(d)**) of which occurred in the MM tests, however, at different rates. Throughout all of the MC specimens, the loading remained near constant after the initial pre-crack failure due to the carbon fibre composite bending, therefore, the opposite end of the specimen lifted slightly throughout the testing. This keeps the load equal to the rate of the load cell displacement throughout the specimen test until the final failure. The extended duration time of the DCB.MC specimens distorts the first two phases of the testing.

Figure 5(e) shows the initial 1 mm displacement graph for the DCB.MC.D specimens, where this magnification allows a clearer view on Phases I and II which is otherwise unseen in **Fig. 5(d)**. The DCB.MC.D.100 specimen showed a very high load gradient initially in Phase I and almost immediately falls after the initial pre-crack failure (see **Fig. 5(e)**). This may have been due to an overlap of the high strength Loctite® EA9466™ adhesive connecting the blocks to the composite, providing an extra bond between the two substrates. Inspection of the DCB.MC.D.100 specimen, found that the occurrence of the initial high loading gradient was backed up to be attributed to the adhesive overlap (**Fig. 5(f)**). The load then appears to remain near constant until the final failure, with very small indications of de-bonding; these occurrences are, however, very clearly shown in the initial stages of the DCB.MC.D load graphs, shown in **Fig. 5(d)**. It was found that MC.B specimens featured sharper initial loading and initial failure than the MC.D specimens (**Fig. 5(g)**). Both sets of specimens show the same trend until the final failure, although the time taken for the brittle adhesive is significantly shorter. This could be due to the adhesive properties or the

method of manufacture, resulting in the time difference. Again, there was a sharp increase and then decrease in load during Phase I and II in **Fig. 5(g)** regarding the DCB.MC.B.65 specimen, which may again be attributed to the high strength Loctite® EA9466™ overlap causing an additional bond. It should be noted that during the insertion of the DCB specimens into the Instron® Model 3382 machine, specimens may have experienced external forces out-with intended testing during alignment of the specimen. Therefore, it was considered that the strength or quality of the adhesive bonds may have been compromised preceding the testing, however were deemed insignificant.

3.2.3 AE analysis

Initial analysis of acquired data showed discrepancies between the AE data files attained and experimental duration. The AE LabVIEW software used to capture the continuous AE data required a buffering period between the 1 second data file captures. Therefore, over the duration of the testing, vital data may have been lost as seen in the loading plot of DCB.MM.D.100 (see **Fig. 6(a)**), where no AE data was recorded for the initial adhesive failure. The lost AE data can be quantified through a simple calculation: $\left(1 - \frac{\text{Total AE record time (s)}}{\text{Total test time (s)}}\right) \times 100\%$. The calculation showed there was an average of 56.03% loss in AE data throughout all experimental tests. This discrepancy in lost data was controllable, where the number of data points taken and the sampling frequency may be reduced to reduce the buffering period between saved data files. However, it has been found that the frequency spectrum ranged the full length of the useful range of the AE sensor, therefore the sampling frequency can only be minimised from 2.5 MHz to 2 MHz. Analysis of the AE data produced from the DCB.MM.D.100 specimen showed an expected steady increase in AE energy towards adhesive failure (see **Fig. 6(b)**), which was in-line with the findings of Ohsawa et al. [32]. When digitally filtered (using Chebyshev Type I filter design) between 100-1000 kHz, the AE signal typically features an increase in maximum AE

amplitude along the time evolution (see **Fig. 6(a)**). The energy in an AE signal is directly related to the AE amplitude; therefore, it can also be stated that the increase in AE amplitude was due to the AE source nearing the AE sensor (see *Section 3.1*). The AE source approached the sensor due to the adhesive failure occurring along the specimen length beginning from the opposing end where the sensor was located. This phenomenon was noticed throughout all DCB test specimens, although especially visible in regards to the DCB.MM.D.100 specimen.

Figure 6(b) excludes the signals created at final fracture measuring at an order of magnitude greater than following greatest AE signals recorded, distorting results. This point was removed due to its insignificance, as the AE signals were created once the specimen had already reached total failure. Prior to adhesive de-bonding (Phases I & II), there appears to be no prominent AE energy from the base signals being generated. The first significant signals were generated within Phase III, however AE signal identification directly at boundary (moment of initial adhesive failure) cannot be ruled out due to the flaws in the AE measuring technique utilised. Visible in **Fig. 6(b)**, varying prominent points of high energy where noticeable changes on the loading graph also occurs. These changes in the loading graph are very significant as they are seen to correlate to different stages of de-bonding, showing capability of the AE technique in regards to adhesive bonds. Displaying maximum AE amplitude of the signals (possible through automated signal processing using MATLAB, while applying loop method to run all data files in a folder for each specimen tested) opposed to AE energy for the individual files of the same specimen, it is clear these same distinctive points along the time evolution are correlated to one another (**Fig. 6(a)**). However, the maximum AE amplitudes highlights signal prominences from the background noise, where a small, though notable pulse (shown with vertical downward arrow, **Fig. 6(a)**) can be seen at the boundary between Phase I and II that is otherwise undistinguishable in the energy plot, in **Fig. 6(b)**. AE amplitudes of interest were designated for further AE analysis. These points

were chosen due to their significant AE magnitude above the background noise and their relation to specific recognisable points on the loading graph that may be of mechanical significance. Where the loading enters Phase III, the adhesive accumulates stress, slowing the rate of loading and may produce an AE response; whereas reduction in loading identifies an adhesive failure. Adhesive stressing and failure have been identified as different potential AE sources to allow a more complete comparison to be discussed; these identified AE files and their respective sources have been compiled into **Table 4**. In addition, it was considered that the white paint, applied to the specimen edge, may be a potential AE source.

Relation of **Fig. 6(a)** to that of Senthil et al. [28] DCB graph, showed very similar characteristics for both load and AE amplitudes created. The load graph displayed the same phases, with correlating AE. The sensor placement, however, in their study was directly above the pre-crack, opposed to the current study where it is at the back of the specimen. This sensor placement explains the differing amplitude magnitudes, where the AE signals at the boundary between Phase I and II are noticeably higher in Senthil et al. [28] representation, where otherwise similar AE signals trends are present. The position of the AE sensor in relation to the initial failure at the pre-crack may introduce an area of large error potential in AE data acquisition as discussed previously in calibration (see *Section 3.1*). Due to the errors carried over from the initial specimen manufacture, the adhesive bonds could potentially feature disbonds or voids [25] and may affect the AE responses acquired at the AE sensing location; where this would potentially result in vital signals being lost. The sensor could be placed closer to the initial failure location (pre-crack) as this has been found to be the most vital location for analysis, where the AE signals of the identified AE sources were at their lowest magnitude. Once the initial failure occurred, the integrity of the specimen was compromised; therefore, more erratic and regular AE signals were generated. A second AE sensor could be introduced to the system, which would allow for a second location to be

monitored and thus correlation between the two could allow further differentiation between AE sources. Therefore, greater accuracy and further analysis could be attained from the comparison of the results. The analysis of the maximum AE amplitudes of all further DCB.MM specimens, found similar recognisable trends, where AE signals appear to first occur after Phase II. However, the AE response found in Phase II of the DCB.MM.D.100 was not visible throughout other DCB.MM testing. Smaller maximum AE amplitudes transmitted at the visibly more drastic changes in loading where adhesive failure occurs. This can be attributed to the location of the sensor at the opposing end of the specimen to where the initial adhesive failure occurs. It can be noted that the disbond's present in the DCB.MM.D.75 specimen created results that moderately compare to Nayeb-Hashemi and Rossettos [25] study, where shorter AE releases compared to the greater distributed signals from the DCB.MM.D.100 specimen.

Figure 6(c) shows the DCB.MM.B.100 load graph with correlating AE maximum amplitudes, where immediate conclusions and comparisons can be drawn regarding the data. Although a slightly differing load graph to the ductile, the same trend of AE signals is present regarding the phases. There were again, no outstanding AE signals at the boundary between Phase I and II. The initial prominent AE signals were created at the start of Phase III, where these observations were realised for all bond qualities for the DCB.MM.B specimens. Bohse and Chen [13] realised this same AE events referring to boundary between Phases II and III as the 'delamination tip'. The signal amplitudes again increase towards the end of failure, supporting previous statements concerning the ductile adhesive for comparing to Senthil et al. [28] study. Initial analysis of the AE data for the DCB.MC specimens confirmed similar trends between the identified maximum AE amplitude responses of the MM and MC specimens. Therefore, it can be stated that AE responses from the DCB specimens gave

detectable AE responses following the Phase II, in the de-bonding process of the experiment, with the exception of the unique occurrence detected in specimen DCB.MM.D.100.

3.3 Three-end notch flexure (3-ENF, Mode-II)

3.3.1 Detection of plastic deformation

Pre-analysis of a specimen featuring a MM un-bonded interface, produced the calculations shown in *Section 2.5*, which were found to correlate with the experimental results. A comparison was drawn between the results of the MM un-bonded interface substrate and the MM.100.B and D specimens (see **Fig. 7(a)**). The deviation from linearity indicates where the substrate was entering its plastic region. It appears that the adhesive steepened the load progression, where following brittle adhesive failure the resultant graph returns to near identical of that without adhesive (see **Fig. 7(a)**). The pre-analysis was effective in providing an estimated loading application for experimentation. Specimens were intentionally taken past their elastic region to extend to gather extra data to gain additional understanding of the standard specimen response for comparison and further discussion.

3.3.2 Loading graphs

Throughout analysis of the 3-ENF testing loading graphs, it was clear that the graphs differ from the DCB experimentation, however, the brittle adhesive graph showing again close comparison to that from Senthil et al. [28] study. Understanding of the various loading traits again, was deemed vital in allowing further discussion concerning the acquired AE responses. The attained loading outputs were split into four phases of mechanical significance. The unique elastic properties of the two adhesives resulted in differing loading traits, especially regarding stage of adhesive failure (see **Fig. 7(b)** and **Fig. 7(c)**). Four

loading graphs for representation have been created to aid in the discussion of the events happening in each Phase for each of the substrate and adhesive specimen combinations.

The loading graphs for the MM.D and MC.D specimen were divided into the following phases: initial roller loading upon the specimen (I); elastic region of the substrates' and adhesive (II); yielding and failure of adhesive (III); and post-final adhesive failure (IV). It becomes apparent that the higher elasticity of the ductile adhesive resists adhesive failure and hence survives throughout the substrates' elastic region. Plastic deformation of the substrates' must occur to induce enough in-plane shear for adhesive failure; this can be identified by the sudden drop at the boundary between Phase III and IV (see **Fig. 7(b)**). This sudden drop or jump was realised in all 3-ENF.MM.D and 3-ENF.MC.D to occur out-with the elastic region of the substrate, for all bond qualities seen in **Fig. 7(c)**, even with the different applied load rates.

All of the 3-ENF tests at the end of Phase I produce a flat line at approximately 0.6 kN (see **Fig. 7(c)**). Comparison with literature would suggest that this could be identified as the transition stage that occurs when the substrate deforms at a constant load equal to that of the collapse load [33]. The collapse load is where the collapse mechanism (indentation or face micro-buckling) of the substrates is initiated. Most of the specimens also show slight fluctuations of load as it increases (**Fig. 7(b)**); this has been determined to be due to the specimen moving within the rollers as they continually adjust to centralise the load, maintaining the programmed rate of displacement. This can be seen throughout all loading graphs for 3-ENF experimentation, especially at the initial stages of the load application. All the MM.D specimens showed a similar loading trend throughout the phases. The load-displacement curve then recovers showing the extending yield of the substrates without adhesive resistance. This happened throughout the MM.D bond qualities, displaying the aluminium substrates yield point occurring before the adhesive failures.

The loading graphs for the MM.B and MC.B specimen were divided into the following phases: initial roller loading upon the specimen (I); adhesive stressing and failure (II); elastic region of the substrates' (III); and the yielding of the specimen substrates' (IV). The brittle properties of the adhesive allow the in-plane shear failure to occur during the elastic stress region of the aluminium substrates, as shown within Phase II (see **Fig. 7(d)**). This is shown in **Fig. 7(e)** with the different load graphs showing an identical failure region (before the elastic region of the substrates'), again at different loading rates between the substrate combinations. However, **Fig. 7(e)** excludes the 3-ENF.MC.B.100 test run, where it experienced unexpected issues when carrying out the test to the designated displacement limitations and all load data was subsequently lost. The point of suggested adhesive failure occurs in Phase II, where the load increases then drops from approximately 1.4 to 1.2 kN (see **Fig. 7(d)**). As the gradient is increasing until apparent failure, the loading profile then seems to return almost to the same as the MM no adhesive specimen (see **Fig. 7(a)**). The ductile adhesive appears to continue causing resistance and thus creating a steeper gradient to also be seen in **Fig. 7(a)**. This occurs until the final adhesive failure, where the loading graph trend follows one similar to the specimen without adhesive. The phases can be verified photographically (see **Fig. 7(f)**), as this allows for the breakdown of results and further analysis. The markings on the edge of the substrate allow observation of the failure mode progression throughout testing, as they move further away from each other. It should be noted that the transition stage for the MC.B and MC.D specimen featured a reduced transition stage (discussed above), which occurs again at approximately 0.6 kN, however for approximately half the duration of the MM specimens. It was deemed that this could be due to the MC specimen not requiring the same force to initiate specimen deformation. Furthermore, the composite properties would aid the absorption of the applied load to the specimen and the elasticity throughout; where this may allow for a higher strain to be undertaken before failure.

3.3.3 AE analysis

Like the DCB results, the loading graphs for each individual test specimen were aligned with the corresponding maximum AE amplitudes. Initial AE analysis of the 3-ENF experiments proved to be less uniform throughout the differing combinations than that of the DCB, due to the mechanical properties of the adhesives with the mode of failure. **Figure 8(a)** shows the AE signals for the 3-ENF.MM.D.100 specimen. The MM.D specimens showed no prominent AE signals in Phase I of the failure for all bond qualities, including the transition stage. This lack of AE signals in Phase I for the MM.D adhesive specimens was consistent with the analysis of the MC.D specimens; however, there was a notable difference where there was a reduced duration of each phase (as discussed above in *Section 3.3.2*).

AE signals of significance were generated in Phase II of the 3-ENF.MM.D failures, with identification of the potential AE sources presented in **Table 5**. The first significant AE signals acquired in 3-ENF.MM.D.100 specimen testing (see **Fig. 8(a)**) can be seen to correlate closely to relate with the centralisation of the rollers. The remainder of the phase shows very little in regards to AE signals being created, with the second substantial AE signals being noticed towards the end of the phase. These observations were reasonably consistent regarding the lack of AE in the two phases, however, the MC specimens showed a noted reduction in accumulative signals. Approaching the apparent adhesive failure, Phase III for all MM.D and MC.D specimens showed the highest accumulation of AE response. The 3-ENF.MM.D.100 specimen shown in **Fig. 8(a)** shows a greater record of AE signals generated before the adhesive failure, where the only other comparison of these signals was found in the 3-ENF.MC.D.75 specimen testing. Most the ductile failures occurred with a ‘jump’, where it was also observed that the AE data for all tests compare accordingly. This analysis shows the applicability of the AE technique in regards to the Mode-II adhesive fracture failure; however, the ductile adhesive specimens cannot be concluded upon definitively in this

instance due to plastic deformation of the substrate before adhesive failure. This would allow generalised conclusions to be made, however, distinction between the AE signals created by the ductile adhesive and the chosen substrates may be impossible for Mode-II experimentation.

The differing load graph profile for brittle adhesives (see **Fig. 8(b)**) compares well with the generated AE signals in Mode-II experimentation as previously discussed for Mode-I results (see *Section 3.2.3*). Like the ductile specimens, Phase I showed no outstanding AE signals, with again the occurrence of the flat line for all specimens tested. The first substantial AE signals for all 3-ENF.MM.B graphs were created within Phase II of the brittle tests; where, as discussed previously there was an obvious load build-up and steep decline insinuating the failure of the adhesive. During the duration of adhesive failure, both the 3-ENF.MM.B.100 and 3-ENF.MM.B.75 specimens showed the highest accumulation of AE signals; whereas, the 3-ENF.MM.B.65 specimen displayed a large proportion of significant maximum amplitude AE signals during and following the adhesive failure. The 3-ENF.MC.B specimens compared relatively well with the 3-ENF.MC.D observations; however, the 3-ENF.MC.B.75 and 3-ENF.MC.B.65 load graphs suggest an initial failure of adhesive that occurred before the transition stage. These initial failures suggest lost AE signals either due to amplitude in comparison to background noise or the system buffering. The 3-ENF.MC.B results showed a single recognisable AE signal at the apparent failure of adhesive, where the loading graph justifies this event with a similarly short-sharp incident.

Following the brittle adhesive failure, there were notable AE responses acquired in the elastic region of the substrate loading. The brittle failure may have resulted in frictional forces occurring between the substrates during further loading where the substrates attempt to move in shear. However, it has previously been discussed that AE responses in the elastic region of the substrate and adhesive loading, may be due to the mechanical processes

occurring during elastic deformation. Furthermore, certain specimens were found to fail out with the elastic region of the substrate and therefore, the adhesive failure may be convoluted within differing AE sources. A variety of the different potential AE sources have been identified for the 3-ENF experimentation to allow a valid, complete comparison to be discussed; these identified AE files and their respective sources have been compiled in **Table 5**. In addition, there have been notable AE responses found at locations where the substrate is loading within the elastic and plastic regions therefore would require analysis to define the AE sources' response.

Repetition of the experimental process would ensure a more complete set of acquired data and provide conformance to the ISO 25217:2009 [3] standard. The ISO 25217:2009 [3] recommends that for Mode-I and Mode-II experimentation, four repeats and five repeats of data for each specimen combination should be acquired, respectively. A more complete set of data would allow valid traits between AE sources to be determined through comparison, and furthermore, reliable AE source data could be averaged for further analysis.

If this investigation could clearly distinguish the AE sources present at the different frequency ranges in the spectrum, then it may be possible to provide a conclusion as to the mechanical phenomena occurring within AE event signals. Filtering of the AE signal into the pre-defined frequency ranges allowed the spectral energy content of the ranges to be defined and hence a comparison of quantified data could be undertaken. Furthermore, spectrogram analysis of AE events would provide a visual description of how the frequency spectrum varies with time evolution. This may identify the time within a signals duration that frequency content arises and for the length of time it occurred. Therefore, this may provide an indication to the occurring mechanical phenomena through an AE signals evolution. The spectral energy found within the frequency domain of the filtered AE signals was generally found to gradually increase along the evolution of time in all experiments; where specimen

DCB.MM.D.100 provides an example in **Fig. 9** for time domain response (**Fig. 9(a)**) and frequency domain response (**Fig. 9(b)**). This was as expected due to *Parseval's* theorem and the general increase in AE amplitude as the AE source approached the AE sensor. However, this was clearly dependent on the amplitude of the selected event and thus discrepancies in this general trend could be identified in the results of certain specimen events' time and frequency domain plots.

The frequency spectra of the experimentation AE signals featured frequency of significant spectral energy, as with the PLB testing of the specimen; however, the AE signals also featured a wider frequency range that spanned the entire useful range of the AE sensor. The spectral energy contained in the higher frequencies (i.e. greater than 400 kHz) were found to be very small in proportion to the areas of significance, however were notable as they were not found span a greater range than found in calibration. The divisions of the frequency ranges into significant and low spectral energy content are displayed in **Table 6** and **Table 7**. It was decided that proportioning the frequency content into percentages would allow normalisation of the data and hence provide a standard comparison. **Figure 10(i)** displays the effect of normalising the individual max amplitude AE events chosen for the six files of data. With a quantified spectral energy proportion, it was more informant in allowing a comparison rather than the visual spectrum displayed in **Fig. 9(b)**. Furthermore, it was clear that the low frequencies have dominant spectral energy content over the higher frequencies; therefore, it was decided to grouping of the higher frequencies into one frequency range of 400-1000 kHz (see **Table 7**) which was sufficient in plotting data thus forth.

As discussed previously in *Section 3.2.3* and *Section 3.3.3* above, the selected maximum AE amplitude events were critically analysed against the experiment duration of the loading graphs to estimate the mechanical phenomena occurring at the selected AE data files. A comparison between the selected AE data files AE source with the spectral energy

proportion may highlight a potential correlation between the mechanical phenomena occurring and the location of energy content in the frequency spectrum. This method of analysis was proven to be effective in some instances; however, the identification of the exact mechanical phenomena occurring was rather difficult without definitive proof in other instances. It would be beneficial to acquire the AE responses during initial pre-analysis experimentation when there was no adhesive bonding incorporated in specimens. This would allow further analysis of the exact AE responses generated with fewer additional potential AE sources acquired in the absence of the adhesive bonding.

Previously, the potential AE sources generated throughout the individual experiments were identified (see **Table 4** and **Table 5**); however, it may be found whether they are of the same or similar frequency spectra through spectral energy proportioning. The six selected AE responses of the DCB.MM.D.100 specimen found a clear comparison of adhesive failure as an acquired AE source for this particular specimen run (see **Fig. 6(a)** and **Fig. 10(ii)**). An exponential trend line was integrated to the plot to determine a correlation between the AE source and the progression of file number. The progression of the file number can also be related to the evolution of time and hence a variation in distance along the specimen length. Therefore, it can be seen from this plot that there was a large difference in where most the spectral energy was situated in the significant frequency range in comparison to the location along the specimen. In addition to this, it was also seen that the high frequency, low spectral energy range was found to increase along the distance of the specimen.

Furthermore, the early adhesive failure of the 3-ENF.MM.B.100 specimens allowed a more clear comparison of the differing AE sources (see **Fig. 8(b)** and **Fig 10(ii)**). Potential AE sources generated post-failure of this specimen adhesive were identified to be either elastic or plastic substrate deformation (see **Table 5**); however, it may be found that they may have the same or similar AE source due to spectral proportioning. There was a large

difference in where most the spectral energy was situated in the significant frequency range in comparison to the location along the loading plot. The chosen files 1-4 are all identified to contain an event within the adhesive failure location; whereas the files 5 and 6 were identified to contain an event within the elastic and plastic deformation regions of the substrates following the adhesive failure, respectively. Therefore, it has been found that there was a difference in the frequency energy proportion dependant on the mechanical phenomena occurring and it may possible to differentiate between AE sources using this analysis method. In addition, similar spectral energy proportion trends could be observed in the adhesive failure as the DCB.MM.D.100 specimen (**Fig. 10(i)**). A trend may also be possible for the adhesive stressing where the difference in the significant frequency range seems to have shifted towards 100-300 kHz (see **Fig. 10(ii)**). However, it was proven to be difficult in confirming the exact mechanical process occurring due to the limited data acquired for comparison of the individual specimen combinations. Further complications arose in the 3-ENF results analysis where ductile adhesive failure occurred during the plastic deformation of the specimen, therefore adding the potential acquisition of another individual AE source (discussed above in this section).

It has been highlighted that there may be the ability to relate and distinguish mechanical phenomena through identification of similarities and differences between the spectral energy proportion of the selected maximum amplitude events. The found consistency with the spectral energy proportion (and hence frequency spectrum) of the identified AE sources within individual specimen, deemed that an average of the acquired proportions for each specimens identified mechanical phenomena may allow valid trends to be recognised with further comparisons. However, the comparison of the averaged spectral energy across the range of the AE experimental data attained for the mechanical phenomena determined

that there may not be a clear relationship between the individual specimens to conclude upon (see **Fig. 11(a)** to **Fig. 11(d)**).

Calibration testing of the specimen confirmed that the frequency spectrum of a consistent, known AE source varied along the length of the specimen. Therefore, this inconsistency in frequency spectrum should be factored into the spectral energy proportion plots in **Fig. 11(a)** to **Fig. 11(d)**, where the AE sources may have been identified correctly, however may have occurred at different lengths along the specimen. The recorded camera footage was deemed to be incapable of giving precise timing of pre-crack failure or debonding with correlation to the load graph data, hence an exact position along the specimen could not be assigned to the selected AE events. However, initial stressing and failure of the adhesive could be assigned to the initial pre-crack stressing and failure; therefore, these AE source locations could be identified accurately as the pre-crack location should always remain consistent and allow a validated location comparison for each individual specimen run. However, the loss in AE data acquisition (discussed above in *Section 3.2.2*) may result in loss of these significant AE responses and therefore would require a more expensive or reliable set-up for AE data acquisition to be designed.

There was a noted difference in frequency spectra of mechanical phenomena that occurred through individual specimen experimentation, which was most recognisable through energy spectral proportioning analysis. It was determined that this was due to the change in frequency spectra along the length of the specimen with a stationary AE sensor and hence limited the comparisons that could be drawn as the AE source location shifted along the specimen length. Oskouei et al. [34] and Bohse and Chen [13] introduced location monitoring through incorporation of multiple AE sensors to enable confirmation of exact AE source location. Therefore, implementation of such a technique may improve the identification of the AE source response as the frequency spectrum varies at different lengths along the specimen.

Furthermore, incorporation of a mounted strain gauge upon the specimen may allow further comparisons with loading data and AE responses to solidify determination of the exact mechanical phenomena. Benmedakhene et al. [26] previously discussed this possibility and determined that specimen featuring two strain gauges (one on specimen face and one through the crack tip thickness) improved the ability to detect crack initiation.

3.4 Outlook

The ‘Testing of Adhesive Bonds’ chapter in the ‘Adhesive Technology Handbook’ by Ebnesajjad and Landrock [35] reveals numerous various testing methods about particular ASTM standards, including some recent literature review [e.g. 2], which highlights the vast topic and importance of mechanical testing concerning adhesive bonds. For relative comparison to other pieces of literature, the approved standards provide a useful guide on the available procedures and experimental set-ups. In addition, conformance to a standard should be specified within all previous literature. However, following an investigation, it becomes apparent that there are no specified requirements for specimen dimensions and procedures, only guides and dimensional measurement methods.

The strength of an adhesively bonded structure can be significantly affected by the presence of a crack and can be usually substantially lower than the strength of the undamaged joints. To avoid catastrophic failure, it can be recommended that one must evaluate the load carrying capacity that will exist in the potentially cracked adhesive joint structure throughout its expected service life. Therefore, the load carrying capacity of a degraded adhesive joint structure is the residual strength of that structure and it is a function of material toughness, crack size, crack geometry and structural configuration. The quality and durability of such adhesive joint or structures have not been extensively characterised experimentally to date. Further, the advancement of increased joint strength (and degradation over years of use)

poses a problem in that there is no well-established experimental methodology to measure it especially for *in-situ* industrial conditions. Further, a link between data from characterisation tests sets and the reliability assessment of these materials is still lacking, especially in terms of remaining service life or re-use applications. Any future work therefore should address the prediction of durability and quality of adhesive joints used for structural rehabilitation, and which can provide a first step in the development of a procedure for assessment of reliability. As seen from the investigation, other AE characteristics (e.g. counts, threshold, rise time, decay time, duration, etc.) were not analysed in this study as the key aim of this investigation was to correlate bond quality features with potential AE sources and their respective type of failure that could enable this investigation to propose AE as a diagnostic indicator for adhesively bonded joint failure. However, due to the nature of this study, and the combination of potential AE sources along with some overlapping events, it is necessary to develop an advanced signal processing method to characterise recorded AE signal. It is anticipated that any enhanced evaluation methodologies should predict the adhesive joint strength with high accuracy. Sensor based instrumented measurement and metrology (possibly combined test methodologies, both non-destructive and semi-destructive) is an important proposition for future re-use or recycling of adhesive joint structures. Such structures can provide numerous failure sites and it may become difficult to track and examine the quality or residual strength by conventional standardized tests. To further the understanding of these failures, the techniques used to monitor the constructions must be expanded upon, e.g. AE technique (and possibly combining other techniques, say ultrasonic) to monitor the mechanical behaviour and failure modes of various material combinations that are bonded together using adhesive. Developing a method of utilising such instrumented technique would be beneficial in understanding the exact or near-exact causes of structural integrity change within the material and layered system.

The study of bonded structure failure has been the area of considerable interest over the past few decades. As an example, it is possible that the nuclear industry could readily employ adhesively bonded joints for applications, such as fabrication of some structural elements of power reactors or for the container walls for the long-term storage of radioactive materials including spent fuel [36]. Therefore, it is crucial that the behaviour of adhesively bonded joints under intense radiation fields and/or prolonged irradiations (leading to joint failure) be fully measured before any assurance is made for nuclear applications. Considering all these factors, there still exists a need to identify proper failure criteria for adhesives, including repeatability of tests under same test conditions. It is expected that practically, any specimens prepared will be unique (if prepared individually), and ideally speaking, it can be difficult to maintain the specimens' quality uniform throughout. However, while investigating series of 4-point bending failure of *Al-to-Al* adhesively bonded joints using the same adhesives (brittle: Loctite® EA3430™; ductile: Loctite® AA326™) and 250 μm bond thickness [37], the investigators indicated that under two test runs, there was good agreement between the finite element simulation and the experimental results. These repeatability issue can vary depending on the nature of the adhesive i.e. ductile or brittle, joint geometry, loading conditions and presence of stress singularity areas such as the interface corner where the bond line meets the edge of the joint.

The investigation of residual strength for un-cracked adhesive joint structures is straight forward because the ultimate strength of the joint is the residual strength. A crack in an adhesive joint structure causes a high stress concentration which can result in a reduced residual strength. When the load or stress on such structure exceeds a certain limit, the crack or failure can extend. The crack extension may become immediately unstable and the crack may propagate in a fast-uncontrollable manner causing complete fracture of the adhesive joint component. To characterize the residual strength capability of a given adhesive joint

structure under certain loading conditions, prediction techniques can be developed with a thorough understanding of the complexities involved in evaluating the residual strength [37-38].

4. Conclusions

Main conclusions drawn are as follows:

- a. Adhesive bond area was found to be irrelevant to the acoustic attenuation for the different specimens when the curing process was uniform and complete. However, any voids in the adhesive bond showed an increased AE signal attenuation for all types of adhesive, bond qualities, and substrate combination. Metal-to-composite specimens were found to attenuate the AE signal more than the metal-to-metal specimens. The metal-to-composite specimens were found to have a greater variation in AE energy than the metal-to-metal specimens.
- b. Frequency spectrums were found to shift in spectral energy proportion as the AE source varied along the specimen length for all types of adhesive, bond qualities, and substrate combination. The first significant maximum AE amplitude event for all adhesive types, bond qualities, and substrate combinations were relatable to the delamination tip (initiation of de-bonding). However, it was proved difficult to propose a definitive AE trait for the mechanical phenomena occurring within specific AE event signals, for all adhesive types, bond qualities, and substrate configurations; therefore, all specimen combinations.
- c. The entirety of the DCB (Mode-I) test results followed a trend that allowed the sectioning of the load plots to be split into three distinct Phases: I, II and III. The results found that the DCB.MM.D.65 specimen showed a different failure than the 100% and 75% bond qualities. It was determined that uncured and voided sections of

specimen would result in stick-slip. All DCB.MM.D specimens showed significant signs of delamination on the loading graphs with high elasticity, whereas, the DCB.MM.B specimens maintained a high, constant load before final failure. The DCB.MC tests also conformed with the three distinct phases, although Phase I and II occurred over a shorter period, which could be attributed to the adhesion properties of the CFRP, or the faster loading displacement rate.

- d. All the 3-ENF test (Mode-II) specimens underwent a transition stage at about 0.6 kN and occurs when the substrate deforms at a constant load equal to that of the collapse load. Two separate sets of phases were established for both ductile and brittle adhesives that were true for both MM and MC combinations. The high elastic properties of the Loctite® AA326TM adhesive (ductile) showed a higher loading resistance. The 3-ENF.MM and 3-ENF.MC brittle specimens showed signs of early failure shortly after the transition stage during the elastic region of the substrates. The test also indicated the brittle adhesive had lower elastic properties and loading resistance as recognised by the low failure load. AE identified the failure of the brittle adhesive in regards to the 3-ENF failure mode, with a cluster of significant maximum AE amplitudes occurring at adhesive failure; whereas, the ductile adhesive's failures occurred in substrates' plastic region and therefore introduced another potential AE source.

References

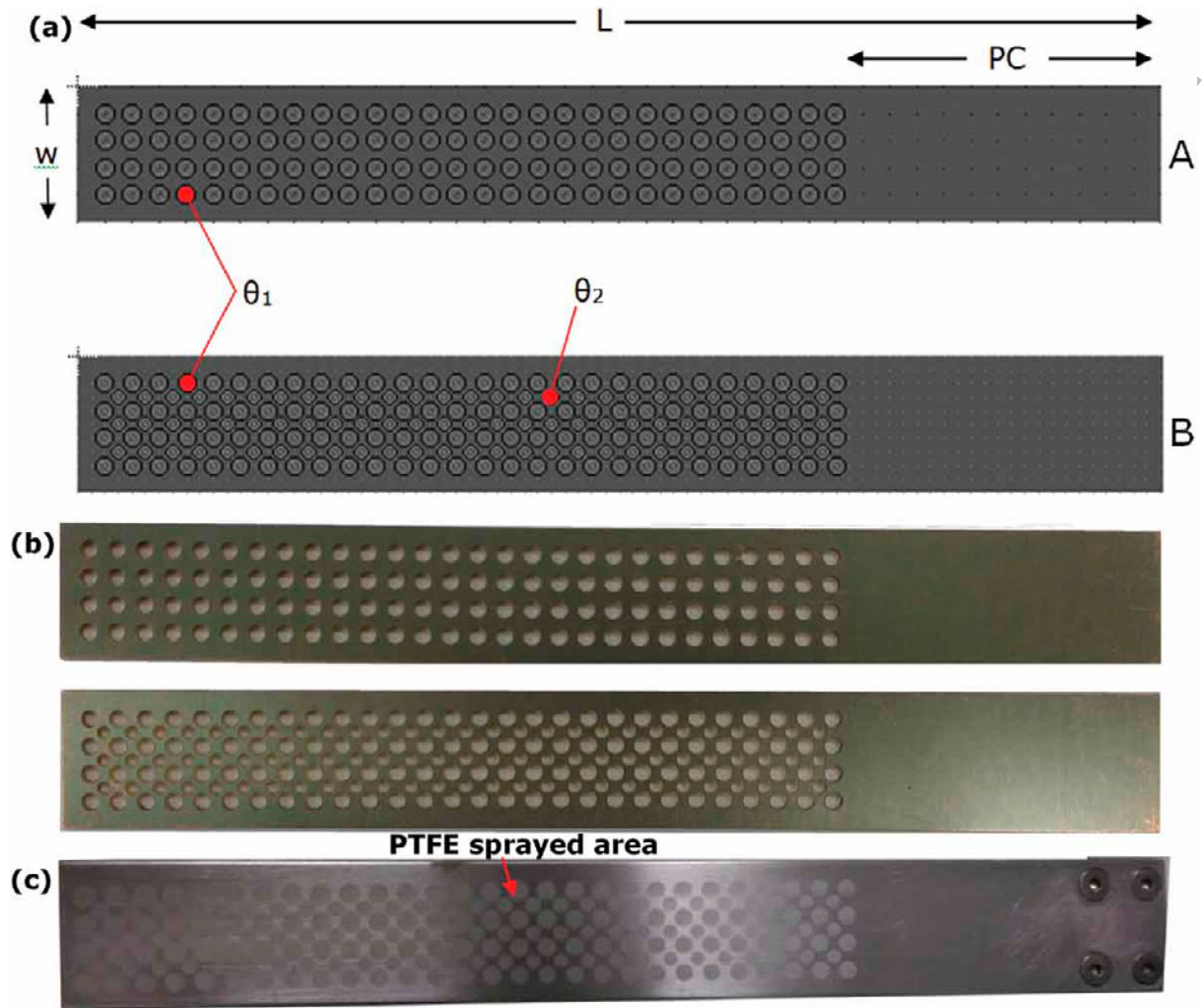
- [1] ASTM, 2015. D907-15: Standard Terminology of Adhesives.
- [2] Chaves, F. J. P., da Silva, L. F. M., de Moura, M. F. S. F., Dillard, D. A., Esteves, V. H. C., *The Journal of Adhesion*. **90**, 955-992 (2014).
- [3] ISO 25217:2009 Adhesives -- Determination of the mode 1 adhesive fracture energy of structural adhesive joints using double cantilever beam and tapered double cantilever beam specimens.
- [4] Adams, R., Cowap, J. W., Farquharson, G., Margary, G. M., and Vaughn, D., *Intl. Journal of Adhesion & Adhesives*. **29**(6), 609-620 (2009).
- [5] Ducept, F., Davies, P., and Gamby, D., *International Journal of Adhesion and Adhesives*. **20**(3), 233-244 (2000).
- [6] Ranade, S. R., Guan, Y., Ohanehi, D. C., Dillard, J. G., Batra, R. C., and Dillard, D. A., *Intl. Journal of Adhesion & Adhesives*. **55**, 155-160 (2014).
- [7] Constante, C., Campilho, R., and Moura, D., *Engineering Fracture Mechanics*. **136**, 292-304 (2015).
- [8] Hasegawa, K., Crocombe, A. D., Coppuck, F., Jewel, D., and Maher, S., *International Journal of Adhesion and Adhesives*. **63**, 124-131 (2015).
- [9] de Moraes, A. B., *International Journal of Adhesion and Adhesives*. **61**, 8-14 (2015).
- [10] Papini, M., Fernlund, G., and Spelt, J. K., *Composites Science and Technology*. **52**(4), 561-570 (1994).
- [11] Campilho, R.M, and da Silva L., *Fatigue and Fracture of Adhesively-Bonded Composite Joints*. **93** (2014).
- [12] Forte, M., Whitney, J., and Schoeppner, G., *Composites Science and Technology*. **60**(12), 2389-2405 (2000).
- [13] Bohse, J., and Chen, J., *Journal of Acoustic Emission*. **18**, 19001-19010 (2001).

- [14] Schuecker, C., and Davidson, B. D., *Composites Science and Technology*. **60**(11), 2137-2146 (2000).
- [15] Schuecker, C., and Davidson, B.D., *Composite Structures: Theory and Practice*, Grant, P. E., and Rousseau, C. Q., Eds., ASTM STP, American Society of Testing of Materials. **1383**, 334-344 (2000).
- [16] Blackman, B., Kinloch, A., and Paraschi, M., *Engineering Fracture Mechanics*, **72**(6), 877-897 (2005).
- [17] Kinloch, A., *Adhesion and adhesives: science and technology*. Springer Science & Business Media. **441** (1987).
- [18] Martin, R., and Davidson, B., *Plastics, Rubber and Composites*. **28**(8), 401-406 (1999).
- [19] de Moura, M., Campilho, R., and Gonçalves J. *International Journal of Solids and Structure*. **46**(6), 1589-1595 (2009).
- [20] Russell, A. J., and Street, K. N., *Toughened Composites*, ASTM STP. **937**, 275-294 (1987).
- [21] Yang, Q., Thouless, M., and Ward, S., *International Journal of Solids and Structure*. **38**(18), 3251-3262 (2001).
- [22] Steinbrecher, G., Buchman, A., Sidess, A., and Sherman, D., *International Journal of Adhesion and Adhesives*. **26**(8), 644-650 (2006).
- [23] Hsu, N., and Breckenridge, F., *Materials Evaluation*. **39**(1), 60-68 (1981).
- [24] ASTM, 1999. E 976-99: Standard Guide for Determining the Reproducibility of Acoustic Emission Sensor Response.
- [25] Nayeb-Hashemi, H., and Rossettos, J. N., *Journal of Acoustic Emission*. 1-14 (1994).
- [26] Benmedakhene, S., Kenane, M., and Benzeggagh, M., *Composites Science and Technology*. **59**(2), 201-208 (1999).

- [27] Bohse, J., *Composites Science and Technology*. **60**(8), 1213-1226 (2000).
- [28] Senthil, K., Arockiarajan, A., and Palaninathan, R., *Engineering Fracture Mechanics*. **154**, 24-42 (2016).
- [29] Boutar, Y., Naïmi, S., Mezlini, S., and Ali, M. B. S., *International Journal of Adhesion & Adhesives*. **67**, 38-43 (2016).
- [30] Schliekelmann, R., *Non-Destructive Testing*. **5**(2), 79-86 (1972).
- [31] Chang, T., Sproat, E. A., Lai, Y. H., Shephard, N. E., and Dillard, D. A., *The Journal of Adhesion*. **60**(1-4), 153-162 (1997).
- [32] Ohsawa, I., Kageyama, K., Tsuchida, Y., and Kanai, M., *Journal of Acoustic Emission*. **21**, 176-186 (2004).
- [33] Tagarielli, V., Fleck, N., and Deshpande, V., *Composites Part B: Engineering*. **35**(6), 523-534 (2004).
- [34] Oskouei, A., Ahmadi, M., and Hajikhani, M., *Express Polym Lett*. **3**(12), 804-813 (2009).
- [35] Ebnesajjad, S., Landrock, A. H., *Adhesives Technology Handbook*. In: Andrew, W., editor. 2014.
- [36] Bonin, H. W., Bui, V. T., Pak, H., Poirier, E., Harris, H., *J Applied Science*. **67**, 37-47 (1998).
- [37] Prathuru, A. K., Faisal, N. H., Jihan, S., Steel, J. A., and Njuguna, J., *The Journal of Adhesion*. 2016. doi: <http://dx.doi.org/10.1080/00218464.2016.1172309>
- [38] Prathuru, A. K., Faisal, N. H., Jihan, S., and Steel, J. A., *Proceedings of the 24th Conference on Computational Mechanics, ACME, 31 March – 1 April 2016, Cardiff, UK*

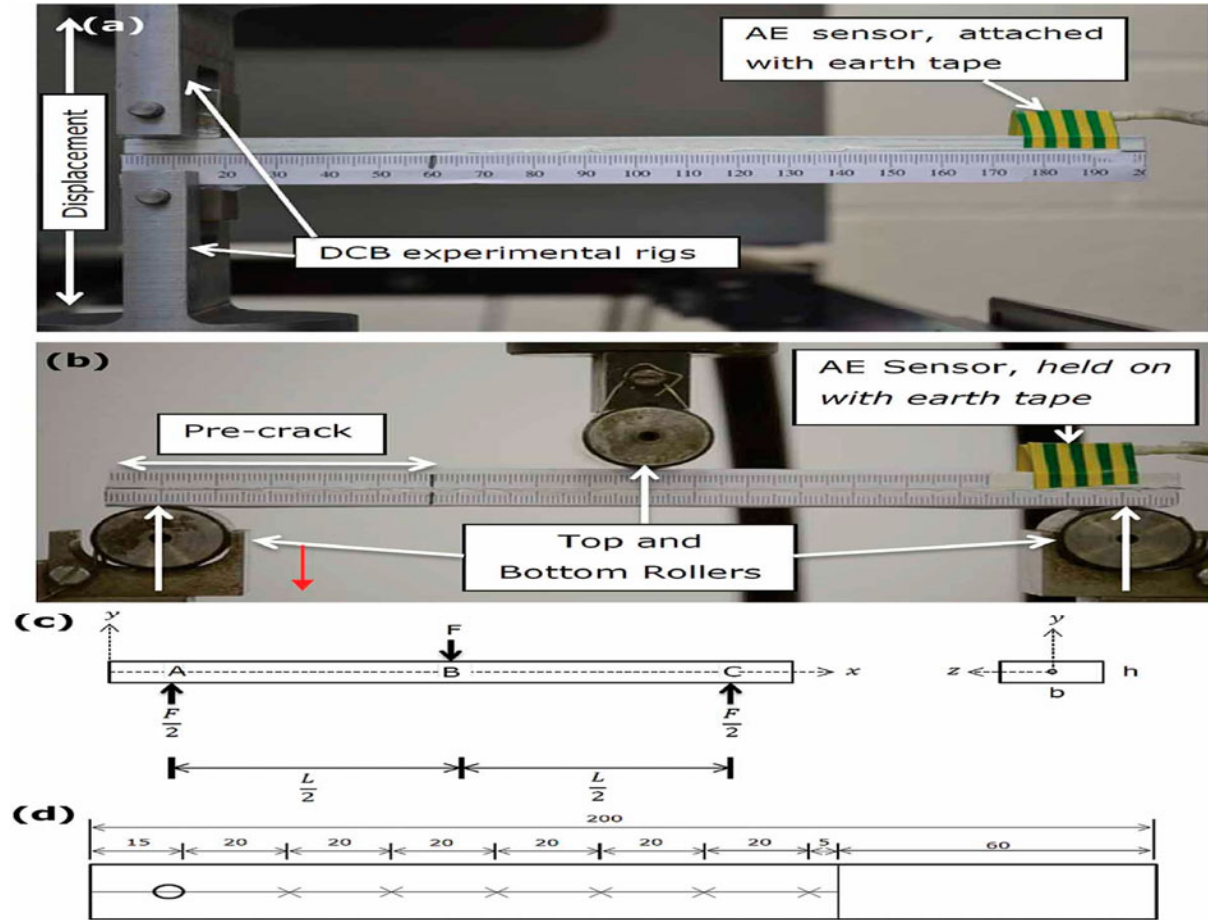
Figure Captions

Fig. 1. Bond area control: (a) masking strip A=25%, masking strip B=35%, where $\theta_1=3.15$ mm and $\theta_2=2.5$ mm, (b) computer numerical control cut templates, and (c) metal specimen with 35% PTFE area reduction.



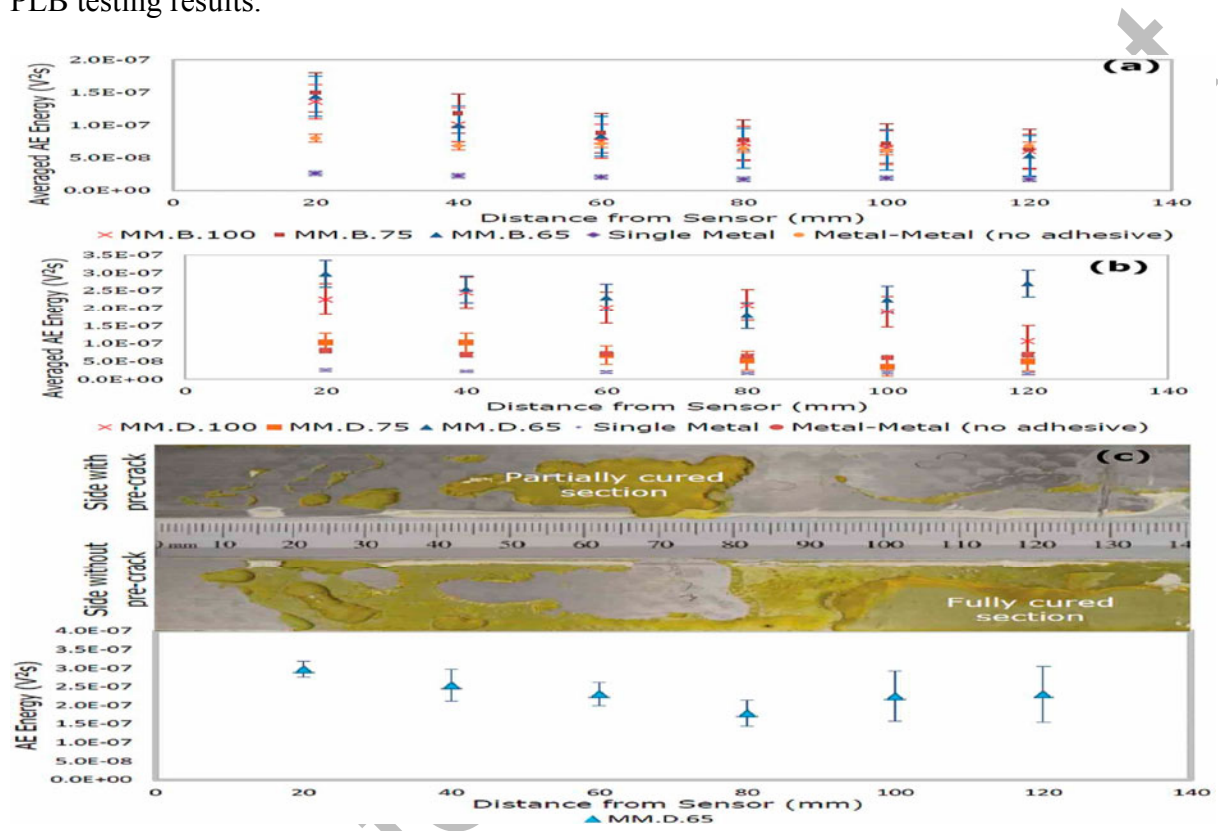
ACQ

Fig. 2. Experimental set-up: (a) Double cantilever beam (DCB, Mode-I) testing (without Instron® 3382 machine), (b, c) 3-end notch flexure (3-ENF, Mode-II) testing, and (d) specimen PLB testing increments.



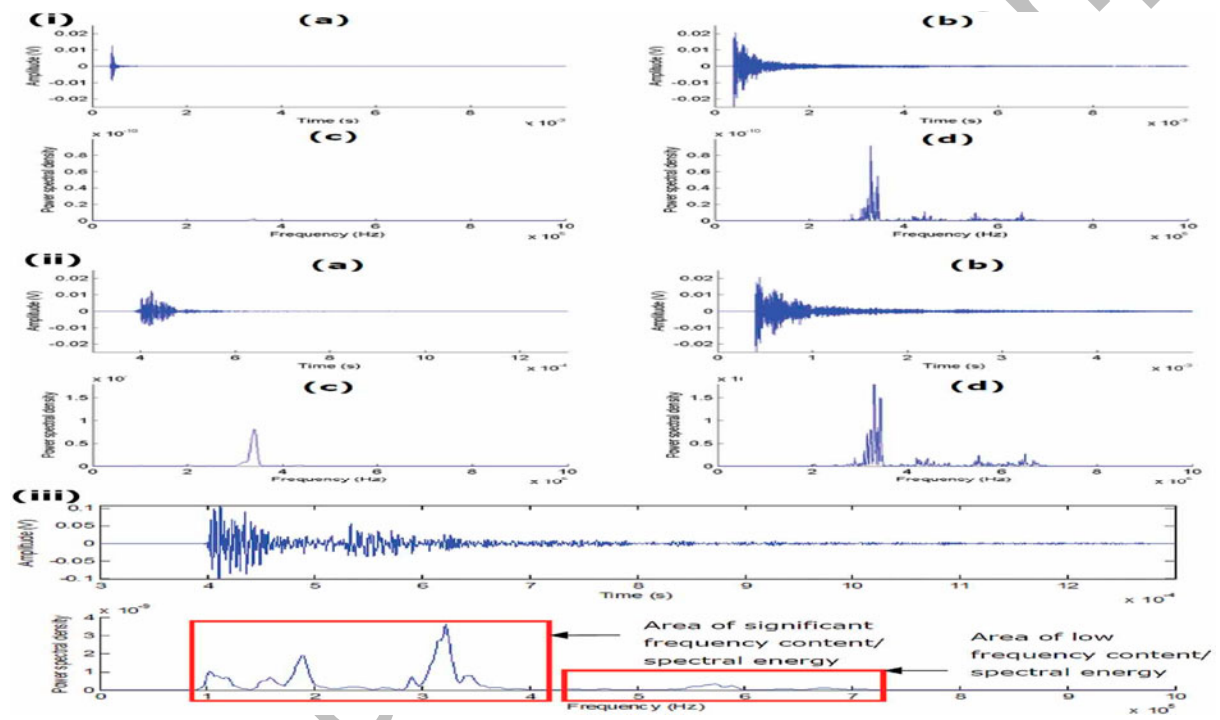
Accepted

Fig. 3. Calibration using PLB test: (a) AE energy on MM.B specimens at different distances from the sensor for each specimen types, (b) AE energy on MM.D specimens at different distances from the sensor for each specimen types, and (c) example when specimen (e.g. MM.D.65) does not fully cure, showing how this may affect the acoustic attenuation of the PLB testing results.



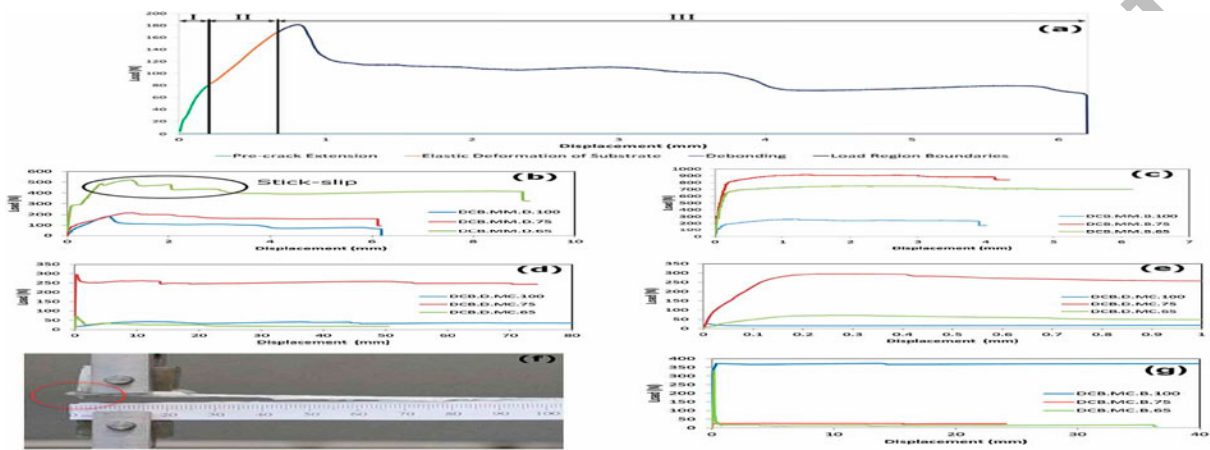
Accepted

Fig. 4. Calibration using PLB test (time and frequency domain signals): (i) comparison of the full window length AE signal response for (a) single composite, time domain, (b) single metal, time domain; (c) single composite, frequency domain, (d) single metal, frequency domain; (ii) comparison of the improved window length AE signal response for (a) single composite, time domain, (b) single metal, time domain, (c) single composite, frequency domain, (d) single metal, frequency domain, and (iii) example of specimen frequency spectrum and the areas of differing frequency content/spectral energy.



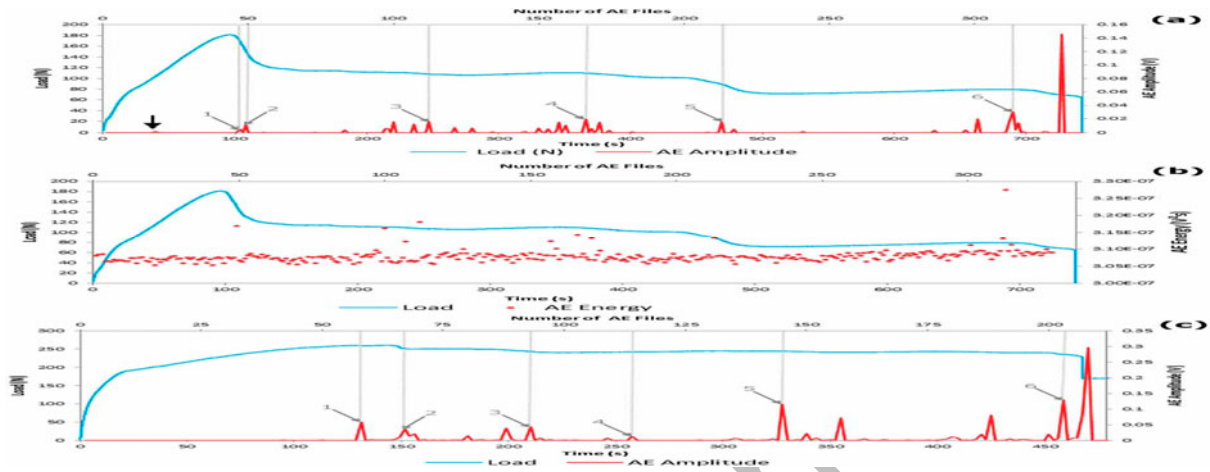
ACCEP

Fig. 5. Double cantilever beam testing (load-displacement profile): (a) DCB.MM.D loading zones, (b) DCB.D.MM loading comparison, (c) DCB.MM.B load comparison, (d) DCB.MC.D loading comparison, (e) DCB.MC.D loading comparison (initial 1 mm displacement), (f) DCB.MC.D.100: overhang of Loctite® EA9466™ adhesive, (g) DCB.MC.B loading comparison, [figures appear in colour in the online version].



Accepted Manuscript

Fig. 6. Double cantilever beam testing (load-time, AE amplitude-time profile): (a) DCB.MM.D.100: load vs. AE amplitude vs. time, (b) DCB.MM.D.100: load vs. AE energy vs. time (excluding final fracture AE signals), and (c) DCB.MM.B.100: load vs. AE amplitude vs. time [figures appear in colour in the online version].

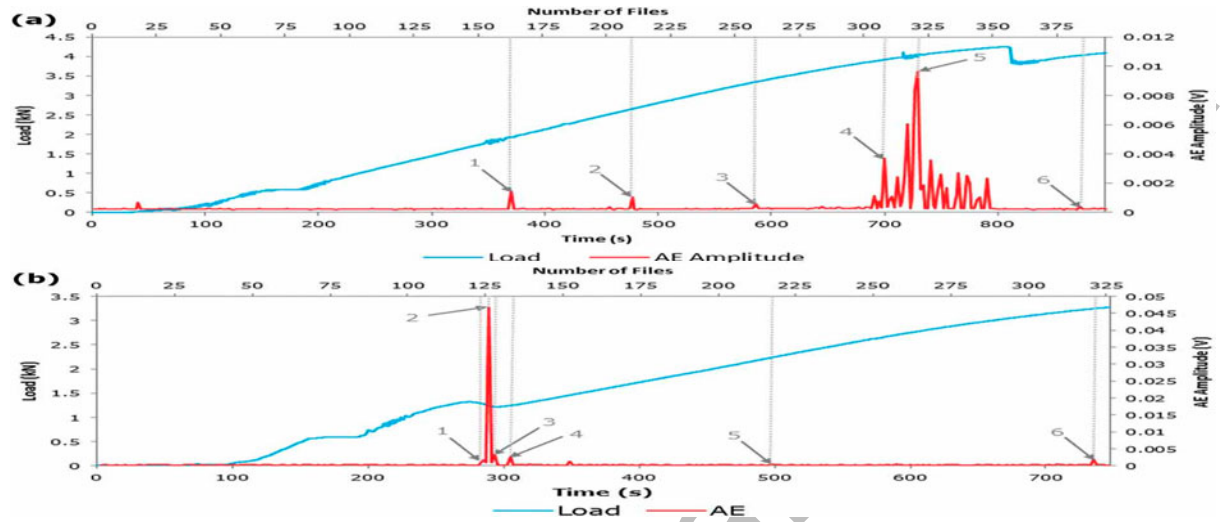


Accepted Manu

Fig. 7. Three-End Notch Flexural (3-ENF) testing (load-time profile): (a) 3ENF: MM (no adhesive) vs. MM.D.100 vs. MM.B.100, (b) load phases of specimen 3ENF.MM.D, featuring magnified indication of specimen slippage, (c) 3ENF.MM/MC.D load comparison, with defined failure region, (d) loading phases of specimen 3ENF.MM.B, (e) 3ENF. MM/MC.B load comparison, with defined failure region, and (f) photographic evidence of typical phase progression of 3-ENF specimen throughout testing procedure [figures appear in colour in the online version].

Accepted Manuscript

Fig. 8. Three-End Notch Flexural (3-ENF) testing (load-time, AE amplitude-time profile): (a) Specimen 3-ENF.MM.D.100: load & AE amplitude vs. time, and (b) specimen 3-ENF.MM.B.100: load & AE amplitude vs. time [figures appear in colour in the online version].



Accepted Manuscript

Fig. 9. Chosen data points for analysis of specimen DCB.MM.D.100, showing their corresponding (a) time domain response; and (b) frequency domain response.

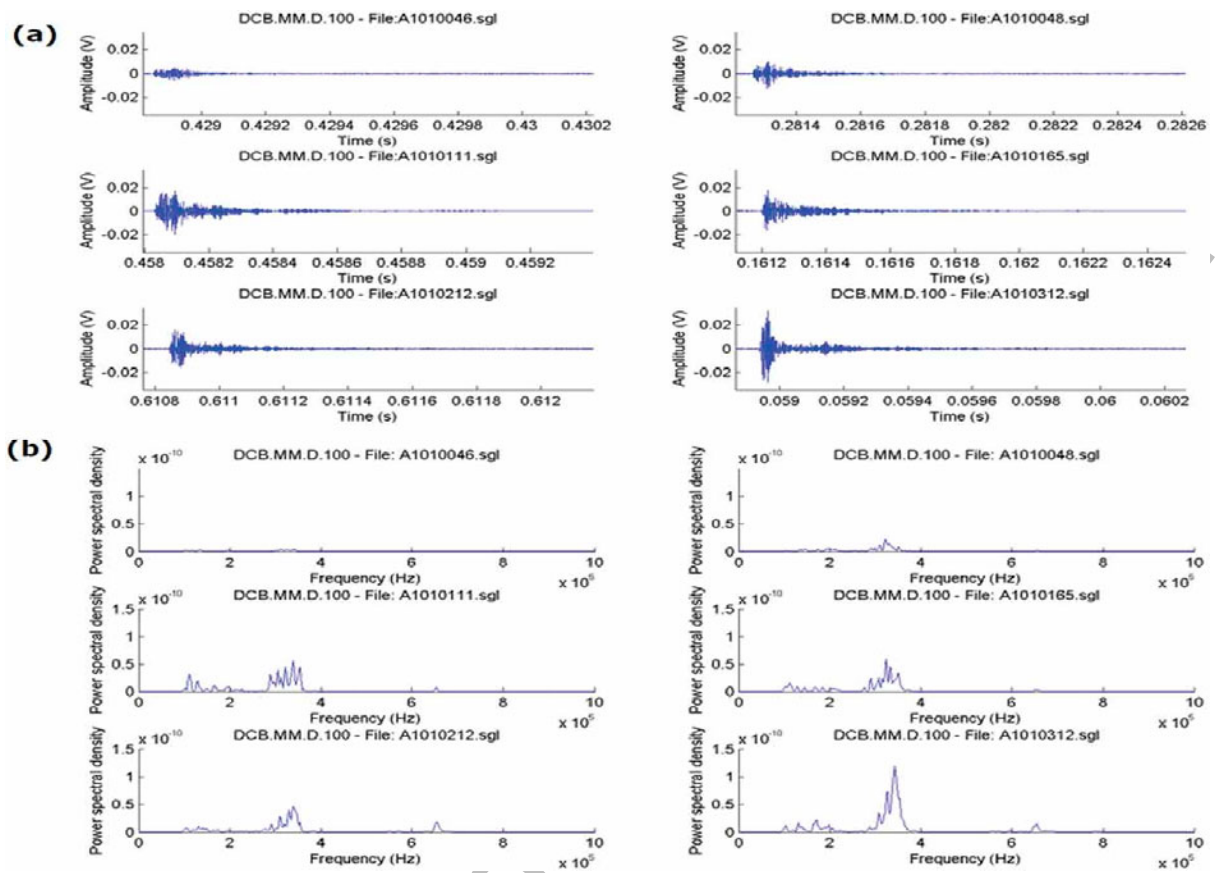
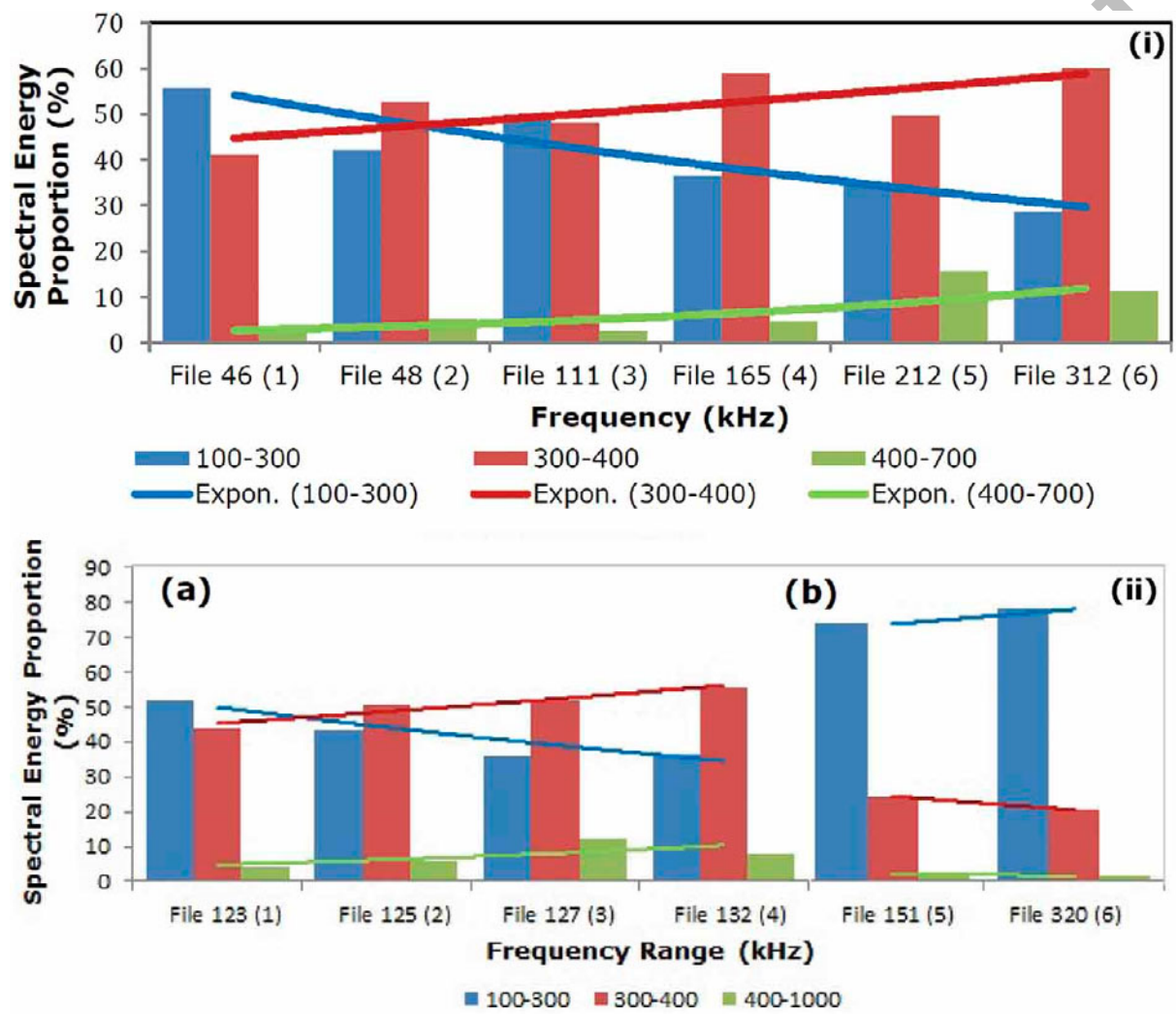
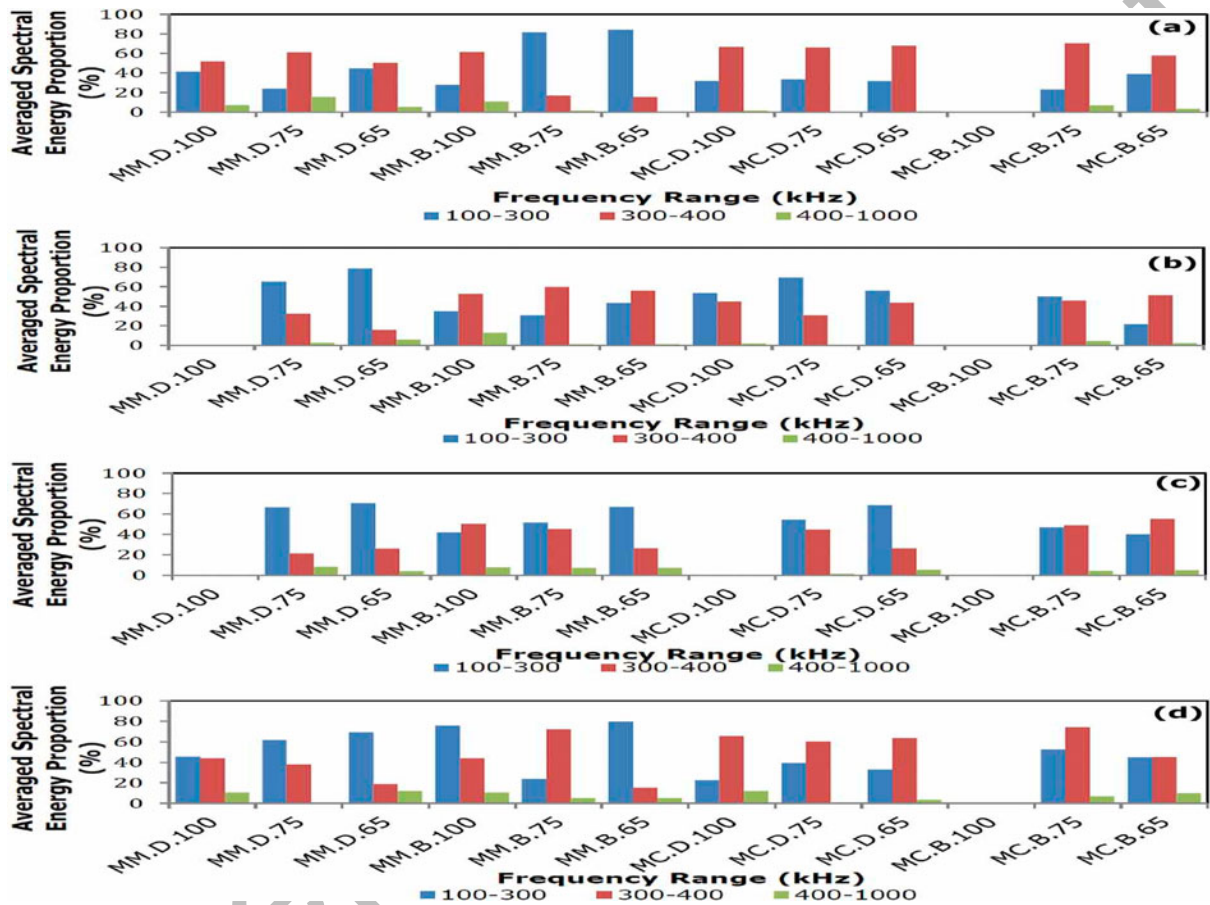


Fig. 10. (i) Example of normalising the frequency content into spectral energy proportion for the individual AE events chosen for the DCB.MM.D.100 specimen, and (ii) comparison of the chosen AE files for 3-ENF.MM.B.100 with their respective spectral energy proportions showing two distinctive in AE sources: (a) adhesive failure; and (b) elastic/plastic substrate deformation [figures appear in colour in the online version].



AC

Fig. 11. Averaged spectral energy: (a) for identified DCB experimental AE source: adhesive failure, (b) for identified DCB experimental AE source: adhesive stressing, (c) for identified 3-ENF experimental AE source: (potential) adhesive failure, and (d) for 3-ENF experimental AE source: elastic/plastic deformation of material [figures appear in colour *in the online version*].



ACCEPTED

Table 1. Adhesively bonded specimen coding system for mechanical testing.

No.	Variables	Double cantilever beam	Three-end notch flexure	DCB test specimen code (one run each)	3-ENF test specimen code (one run each)
1	Test coding	DCB	3-ENF	DCB.MM.D.100	3-ENF.MM.D.100
2	Metal-to-Metal (each metal thickness = 6.37 mm)	MM	MM	DCB.MM.D.75 DCB.MM.D.65	3-ENF.MM.D.75 3-ENF.MM.D.65
3	Metal-to-Composite (metal thickness = 6.37 mm; composite thickness = 1.35 mm)	MC	MC	DCB.MM.B.100 DCB.MM.B.75 DCB.MM.B.65	3-ENF.MM.B.100 3-ENF.MM.B.75 3-ENF.MM.B.65
4	AA 326 TM (Ductile)	D	D	DCB.MC.D.100	3-ENF.MC.D.100
5	EA 3430 TM (Brittle)	B	B	DCB.MC.D.75 DCB.MC.D.65	3-ENF.MC.D.75 3-ENF.MC.D.65
6	Bond area quality	100% 75% 65%	100% 75% 65%	DCB.MC.B.100 DCB.MC.B.75 DCB.MC.B.65	3-ENF.MC.B.100 3-ENF.MC.B.75 3-ENF.MC.B.65

Accepted Manuscript

Table 2. Significant frequency content present within the filtered frequency ranges.

	MM.D	MM.B	MC.D	MC.B
Frequency Range (kHz)	100-400	100-400	100-400	100-400

Accepted Manuscript

Table 3. All frequency content present in the within the filtered frequency range.

	MM.D	MM.B	MC.D	MC.B
Frequency Range (kHz)	100-850	100-800	100-700	100-700

Accepted Manuscript

Table 4. Identified mechanical phenomena for the corresponding AE data file (ref. Fig. 6) used in analysis, acquired from DCB experimentation.

Double Cantilever Beam	File Number					
	1	2	3	4	5	6
MM.D.100	Adhesive Failure					
MM.D.75	Adhesive Stress	Adhesive Failure				
MM.D.65	Adhesive Failure	Adhesive Stress				
MM.B.100	Adhesive Failure	Adhesive Stress	Adhesive Failure	Adhesive Stress	Adhesive Failure	Adhesive Failure
MM.B.75	Adhesive Stress	Adhesive Stress	Adhesive Stress	Adhesive Failure	Adhesive Failure	Adhesive Failure
MM.B.65	Adhesive Stress	Adhesive Stress	Adhesive Stress	Adhesive Failure	Adhesive Failure	Adhesive Failure
MC.D.100	Adhesive Stress	Adhesive Stress	Adhesive Failure	Adhesive Failure	Adhesive Failure	Adhesive Failure
MC.D.75	Adhesive Failure	Adhesive Failure	Adhesive Failure	Adhesive Stress	Adhesive Failure	Adhesive Failure
MC.D.65	Adhesive Stress	Adhesive Failure	Adhesive Failure	Adhesive Failure	Adhesive Failure	Adhesive Stress
MC.B.100	N/A	N/A	N/A	N/A	N/A	N/A
MC.B.75	Adhesive Failure	Adhesive Failure	Adhesive Failure	Adhesive Failure	Adhesive Stress	Adhesive Stress
MC.B.65	Adhesive Failure	Adhesive Stress	Adhesive Stress	Adhesive Failure	Adhesive Stress	Adhesive Stress

Accepted Manuscript

Table 5. Identified mechanical phenomena for the corresponding AE data file (ref. Fig. 8) used in analysis, acquired from 3-ENF experimentation.

3-End Notch Flexure	File Number					
	1	2	3	4	5	6
MM.D.100	Roller Contact/Slip	Substrate	Substrate	Substrate	Substrate	Roller Contact/Slip
	Elastic Region	Elastic Region	Plastic Region	Plastic Region	Plastic Region	Plastic Region
MM.D.75	Substrate	Potential Adhesive Failure	N/A	N/A	N/A	N/A
	Plastic Region	Potential Adhesive Failure	N/A	N/A	N/A	N/A
MM.D.65	Substrate	Substrate	Potential Adhesive Failure	Potential Adhesive Failure	Potential Adhesive Failure	Potential Adhesive Failure
	Elastic Region	Plastic Region	Potential Adhesive Failure	Potential Adhesive Failure	Potential Adhesive Failure	Potential Adhesive Failure
MM.B.100	Adhesive Failure	Adhesive Failure	Adhesive Failure	Adhesive Failure	Substrate	Substrate
	Elastic Region	Elastic Region	Elastic Region	Elastic Region	Elastic Region	Plastic Region
MM.B.75	Adhesive Failure	Adhesive Failure	Adhesive Failure	Substrate	Substrate	Substrate
	Elastic Region	Elastic Region	Elastic Region	Elastic Region	Elastic Region	Plastic Region
MM.B.65	Adhesive Failure	Adhesive Failure	Adhesive Failure	Adhesive Failure	Substrate	Substrate
	Elastic Region	Elastic Region	Elastic Region	Elastic Region	Elastic Region	Plastic Region
MC.D.100	Substrate	N/A	N/A	N/A	N/A	N/A
	Elastic Region	N/A	N/A	N/A	N/A	N/A
MC.D.75	Substrate	Substrate	Substrate	Potential Adhesive	Potential Adhesive	Substrate
	Plastic Region	Plastic Region	Plastic Region	Plastic Region	Plastic Region	Plastic Region
MC.D.65	Substrate	Potential Adhesive	Substrate	Substrate	Potential Adhesive	Substrate/Adhesive
	Plastic Region	Plastic Region	Plastic Region	Plastic Region	Plastic Region	Plastic Region
MC.B.100	Potential Adhesive	Potential Adhesive	Substrate	Substrate	Substrate	Substrate
	Elastic Region	Elastic Region	Plastic Region	Plastic Region	Plastic Region	Plastic Region
MC.B.75	Adhesive Failure	Substrate	Substrate	Substrate	N/A	N/A
	Elastic Region	Elastic Region	Plastic Region	Plastic Region	N/A	N/A
MC.B.65	Adhesive Failure	Adhesive Failure	Substrate	Substrate	Substrate	Roller Contact/Slip
	Elastic Region	Elastic Region	Elastic Region	Elastic Region	Plastic Region	Plastic Region

Table 6. Significant spectral energy content within the filtered frequency ranges.

Experimentation Mode	Frequency Range (kHz)			
	MM.D	MM.B	MC.D	MC.B
DCB	100-400	100-400	100-400	100-400
3-ENF	100-400	100-400	100-400	100-400

Accepted Manuscript

Table 7. Low spectral energy content within the filtered frequency ranges.

Experimentation Mode	Frequency Range (kHz)			
	MM.D	MM.B	MC.D	MC.B
DCB	400-1000	400-1000	400-1000	400-1000
3-ENF	400-1000	400-1000	400-1000	400-1000

Accepted Manuscript